Current Opinion in Solid State and Materials Science 26 (2022) 100976

Contents lists available at ScienceDirect

Current Opinion in Solid State & Materials Science

journal homepage: www.elsevier.com/locate/cossms

# On amorphization as a deformation mechanism under high stresses

Hosni Idrissi [a,b], Philippe Carrez [c], Patrick Cordier [c,d,*]

[a] Institute of Mechanics, Materials and Civil Engineering (IMMC), UCLouvain, B-1348 Louvain-la-Neuve, Belgium
[b] EMAT, University of Antwerp, Groenenborgerlaan 171, B-2020 Antwerp, Belgium
[c] Univ. Lille, CNRS, INRAE, Centrale Lille, UMR 8207 - UMET - Unité Matériaux et Transformations, F-59000 Lille, France
[d] Institut Universitaire de France, F-75005 Paris, France

ARTICLE INFO

*Keywords:*
Amorphization
Mechanical instability
Plasticity
Deformation mechanism

ABSTRACT

In this paper we review the work related to amorphization under mechanical stress. Beyond pressure, we highlight the role of deviatoric or shear stresses. We show that the most recent works make amorphization appear as a deformation mechanism in its own right, in particular under extreme conditions (shocks, deformations under high stresses, high strain-rates).

## 1. Introduction

The practical ability to shape materials into desired forms by deforming them represented a major technological revolution in human history. However, it is only since a hundred years that we have the theoretical tools to understand and control the processes of plastic deformation of solids. Most structural materials, among which metals, are crystalline. That is to say that the atomic arrangement is, above all, characterized by short and long-range order which is not very compatible with the capacity to undergo large strains (like fluids). Most crystal plasticity theories involve crystal defects. Only a small fraction of atoms in the crystal have local arrangements which deviate from perfect crystal. Their motion carries plastic strain. These defects are point defects, line defects (dislocations, disclinations, disconnections), grain boundaries, twins. More recently, it has been shown that phase transformations can be controlled to shape materials. The development of TRIP steels since the 90′s is an illustration of this. In this article we consider a phase transformation that is a bit particular, since it is always out of equilibrium: *stress(pressure)-induced amorphization*. The local loss of long-range order radically changes the mechanical properties of solids. At first considered as a curiosity, this phenomenon is emerging as a deformation mechanism in its own right. In the following we review the current understanding of this phenomenon with emphasis on the aspects related to mechanical properties.

## 2. The many routes from crystalline to amorphous state

Compared to crystals, amorphous solids lack long-range translational and orientational order. The contribution of the configurational entropy associated with this disorder is not sufficient to stabilize the amorphous phase with respect to the crystalline phase. Glasses are a type of amorphous solids which occur naturally in nature, mostly resulting from igneous processes. Obsidian is a natural volcanic glass produced when lava extruded from a volcano cools fast enough to prevent crystallization. Tektites are natural glasses formed from molten ejecta resulting from a meteorite impact. After ejection, the molten droplets (ranging in size from millimeters to centimeters) rapidly cool either during the ballistic flight or when hitting the ground. These natural glasses have been used by man from the earliest times to fabricate artifacts. Appeared some 4500 years ago in the middle east during the Bronze age, man-made glass preceded iron and is among the earliest man-made materials [129]. In all these cases, glass is formed from cooling a liquid at a rate fast enough to hinder crystallization kinetically. When a liquid, which represents a well-defined phase in internal thermodynamic equilibrium is cooled, equilibrium can only be maintained through relaxation mechanisms which may involve diffusion. However, as temperature decreases, these processes become less efficient, and a disordered configuration may be frozen in before crystalline order emerges. The route from crystal to amorphous is here indirect, involving an intermediate state: the liquid. It is thus melting which destabilizes the crystalline state. Melting is probably the oldest studied phase transformation. It occurs at the temperature at which the free energy of the

* Corresponding author at: Univ. Lille, CNRS, INRAE, Centrale Lille, UMR 8207 - UMET - Unité Matériaux et Transformations, F-59000 Lille, France.
*E-mail address:* Patrick.cordier@univ-lille.fr (P. Cordier).

https://doi.org/10.1016/j.cossms.2021.100976
Received 10 September 2021; Received in revised form 11 December 2021; Accepted 14 December 2021
Available online 13 January 2022

crystalline phase equals that of the liquid. In practice one observes that melting nucleates on external surfaces, or possibly on internal defects such as dislocations or grain boundaries. Lindemann [80] proposed that at the melting point, the amplitude of atomic vibrations is so large that atomic spheres overlap. Gilvarry [42] further gave a firmer basis to Lindemann's model by postulating that, at fusion, the root mean square amplitude of atomic vibrations reaches a critical fraction $\delta$ of the distance of separation of nearest neighbor atoms. Melting of many crystalline solids occur for $0.07 \leq \delta \leq 0.15$.

If, beyond melting, a compound is vaporized, sublimation by condensation on a cold surface may represent another route to obtain amorphous thin films [5].

Some natural materials have provided evidence for other routes to form amorphous solids. The case of diaplectic glasses found in meteoritic craters will be described below. It was also reported in 1893 by Broegger [17] that some minerals, originally crystalline had developed over geological times some characteristics of amorphous materials. He named them metamict phases from the Greek for "mix otherwise". It was later suggested [56] that disordering resulted from the action of alpha particles and recoil nuclei. The experimental demonstration that crystalline materials can be amorphized by irradiation was made in 1962 by Bloch [9] who amorphized $U_6Fe$ by fast fission fragments. This phenomenon affects mostly actinide containing oxides and silicates. The same effect can be produced by electron beams either in a scanning, or in a transmission electron microscope (*e.g.* [66]).

Some high-pressure phases cannot be quenched under ambient conditions and amorphize when the pressure is released. This is the case for davemaoite, the perovskite phase of $CaSiO_3$, when the pressure drops below *ca.* 10 GPa [155] and for the (Mg, Fe)$SiO_3$ post-perovskite phase [61] stable at conditions of the base of the lower mantle of the Earth only. Some high-pressure phases can be quenched at ambient pressure. However, further heating often leads to amorphization rather than to the formation of the stable crystalline phase. This is the case for coesite and stishovite (two high-pressure polymorphs of silica) when heated at moderate temperature (300–1000 °C) at ambient pressure [116,31]. The same phenomenon is observed in Cd-Sb when the high-pressure phase rapidly cooled to liquid nitrogen under pressure is simply brought back to ambient pressure and temperature [77].

In the following we will put the emphasis on mechanically-driven crystal to amorphous transformation.

## 3. Pressure induced amorphization

Isotropic and x-ray amorphous minerals of quartz, plagioclase and alkali-feldspar composition were commonly found among shock products of terrestrial [118,19,39,119] and lunar [20] impact environments. Textural evidence led to the distinction between two types of amorphous material in these samples. One, showing indices of flow and vesicles, was interpreted as resulting from melting and quench. However, other amorphous materials appeared as isotropic phases preserving all morphological features of the previous crystalline phase, such as grain morphologies. They were called diaplectic (from the Greek word *diaplesso* = to destroy by striking) glass by Engelhardt *et al.* [38]. The refractive index of diaplectic quartz glass is higher than that of synthetic silica glass, decreasing with increasing shock intensity. Similarly, the density of diaplectic quartz glass is higher than the density of synthetic quartz [156]. The origin of diaplectic glass was discussed as a reversion product of a dense high-pressure polymorph [33] *e.g.* stishovite in the case of quartz, or as a result of heterogeneous deformation in the mixed phase regime (Fig. 1) indicated by the Hugoniot [46].

Indeed, diaplectic glasses have been produced experimentally and observed in recovered products of shock experiments [88,95,120,157]. Similar shock features and occurrence of diaplectic glass was reported from nuclear explosions ([114–115,13,29], Fig. 2a). The study of shock microstructures in minerals, and in particular in quartz, has received renewed interest in the context of the Cretaceous/Paleogene (K/Pg, called at that time K/T for Cretaceous/Tertiary) mass extinction controversy [2]. One of the clues attributed to a meteorite impact is the presence of quartz grains with characteristic planar deformation features (PDFs) in the K/Pg boundary sedimentary layer [11]. These PDFs occur as multiple sets of parallel, thin lamellae parallel to rational low index planes. The most frequent orientations are rhombohedral $\{10\bar{1}n\}$ (n = 1–4) planes, the basal plane and $\{11\bar{2}n\}$ (n = 0–2) planes. The orientation distribution depends on the peak stress, and on the direction of shock propagation [74].

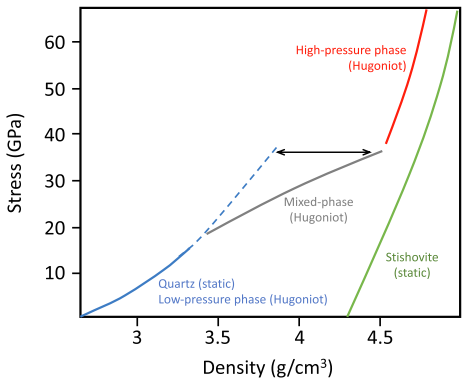


**Fig. 1.** Shock Hugoniot curve for quartz (adapted from [131]). Blue dashed line is an extrapolated equation of state fit to the 300 K quartz data. The 300 K static compression data for stishovite are represented by the green line.

Transmission electron microscopy (TEM) studies of PDFs from natural impact sites revealed that, except those in the basal plane which consist in Brazil twins, unaltered PDFs are in fact amorphous lamellae [153,154]. The amorphous nature of PDFs was established without ambiguity in experimentally shocked quartz [47,48,49,73] showing that PDFs occur frequently in orientations perpendicular to the shock front (Fig. 2b). This led Goltrant *et al.* [154] to propose a model (Fig. 3) where PDFs accommodate the compressional deformation at the shock front (*i.e.* the interfaces where uncompressed and compressed crystals must match).

Such a mechanism may seem paradoxical since a pressure-induced transformation is supposed to induce a negative volume change. The key to the phenomenon lies in the high compressibility of amorphous materials which allows them to be denser than the crystal under high-pressure. Diaplectic glass forms in increasing quantities from 10 to 40 GPa, with melting occurring above 50–60 GPa. The amount of glass formed also increases with temperature suggesting that amorphization is a thermally activated process with an apparent activation energy estimated by Gratz *et al.* [49] to be < 60 kJ/mol. From the Hugoniot, the amount of compressional deformation can be estimated to reach $\Delta V/V \sim 15\%$ at 40 GPa (Fig. 1).

Shock induced amorphization has been observed in silicates as well, for instance olivine shocked and recovered from peak pressure of about 56 GPa showed amorphous zones [67]. This was the first report of olivine glass. The isolated $SiO_4$ tetrahedra of olivine rearrange easily to form the crystalline structure, and generating glassy olivine from quenching of the melt is thus very difficult. Feldspars occurring frequently in crustal rocks of differentiated bodies in the solar system, the transformation of plagioclase into diaplectic glass (called maskelynite, [88]) has been widely used as a shock indicator [121]. As in quartz, feldspars exhibit a progressive amorphization under pressure with formation of PDFs above 18 GPa. This threshold decreases to 15 GPa when the initial temperature is raised from 25 °C to 750 °C [64]. PDFs in plagioclase exhibit a variety of orientations including (001), (021), $(1\bar{1}1)$ and $(1\bar{3}1)$ [64]. Molecular dynamics (MD) simulations are very well suited to investigate the behavior of materials under high strain rates. Using this approach, it was shown that fcc metallic nanorods subjected to strain rates above $2.10^{10}$ $s^{-1}$ undergo amorphization (called

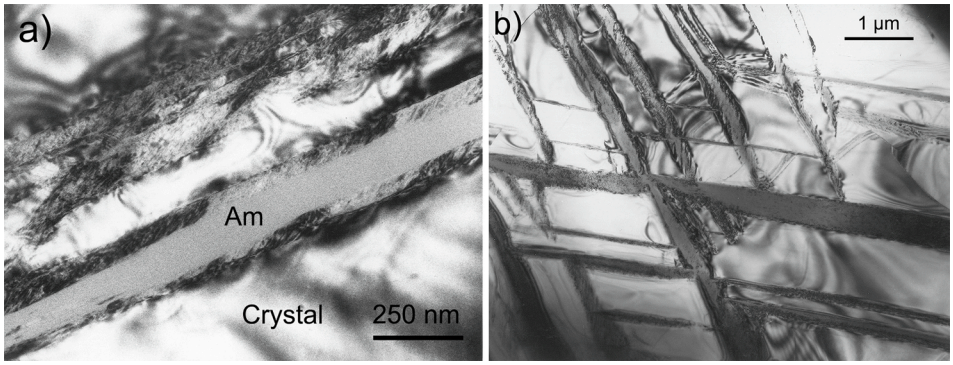


**Fig. 2.** Planar deformation features (amorphous lamellae) induced by shock in quartz. a) granodiorite from the Sedan Nuclear test (100 kT) site (1962) [29]. b) Quartz single crystal experimentally shocked at 23 GPa, −170 °C [49].

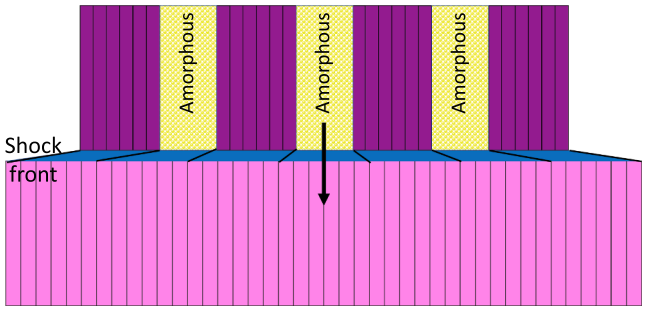


**Fig. 3.** Schematic representation of the volumetric accommodation at the shock wave front by thin lamellae of dense amorphous silica. Modified after [154].

momentum-induced amorphization) and deform nonlinearly in a plastic flow manner [16,65,158]. Strains up to several tens of percent are reached in these numerical experiments.

This brief description of shock metamorphism in quartz and other mineral phases shows that the study of amorphization induced by (dynamic) pressure is almost 60 years old. However, the paper by Mishima *et al.* [90] on ice is generally considered to be the starting point of the field of research that has since been named "pressure-induced amorphization". Pressure-induced amorphization (PIA) has since been the subject of several detailed and high-quality reviews [159–161]. It is not the intention here to duplicate these articles. We summarize only the aspects most relevant to our interest: deformation, here through compression. Mishima *et al.* [90] compressed ice $I_h$ to 1 GPa at 77 K. Instead of obtaining the ice VI polymorph predicted by the phase diagram, the hexagonal ice became amorphous. This discovery was quickly followed by the observation of the amorphization under static pressure of quartz [59,57,68] which led to further detailed studies. Particular attention was paid to the study of the structural modifications leading to the amorphization of quartz under pressure. Hazen *et al.* [57] observe that $SiO_4$ tetrahedra are not affected during compression, which essentially results in a dramatic decrease of the Si-O-Si angle and the distance between the tetrahedra. This observation was confirmed theoretically by Chelikowski *et al.* [22]. The threshold of amorphization coincides with Si-O-Si angles below 120° while the oxygen sublattice approaches a close-packed cubic arrangement (bcc) as it had already been underlined by Sowa [162] and further shown theoretically by Binggeli *et al.* [8]. Stolper and Ahrens [122] point out that in glasses and melts the decrease in Si-O-Si angles can be accompanied by a change in Si coordination to values higher than 4 and propose that the same may be true in crystal-amorphous transformations. This hypothesis is supported by the calculations of Wentzcovitch *et al.* [138] who theoretically identified, under pressure, a metastable phase with a mixture of edge-sharing $SiO_6$ octahedra and $SiO_5$ cuboids. This structural interpretation is not universal, because minerals with a three-dimensional framework of $SiO_4$ (like quartz or feldspars, *e.g.* anorthite [139]) are not the only ones to amorphize under pressure. It was indeed observed that olivine, which presents a quasi-compact oxygen sub-lattice and isolated tetrahedra, also amorphizes under pressure [37,53,108,163]. In their recent study involving reaction pathway sampling based on first-principles calculations, Guan *et al.* [50] also show that, in olivine, the silicate $SiO_4$ tetrahedron moves as a molecular entity during the whole pressure-induced solid phase transformation. Pressure induced amorphization has also been observed in layered silicates, serpentines [84,85], who also reported amorphization of portlandite). Quasicrystals [1] or covalent bonded materials (silicon, [140]; gallium arsenide, [76]) also become amorphous under pressure demonstrating that a large variety of crystal structures exhibit this behavior.

The first report of pressure induced amorphization of ice $I_h$ by Mishima *et al.* [90] was interpreted as a metastable melting event [91]. For some materials, the Clapeyron slope for melting $(dT_m/dP)$ is negative (Fig. 4). This implies that an isothermal compression can result in a point where the melting temperature extended metastably is lower than the compression temperature. This interpretation has allowed a reasonable account of the observations of Mishima *et al.* [90] on ice and of Hemley *et al.* [59] on quartz.

One of the limitations of the thermodynamic approach is that amorphization is also determined by kinetic factors. It is now quite clear that amorphization only occurs if the nucleation and growth of the crystalline phase at equilibrium is prevented. These aspects can be

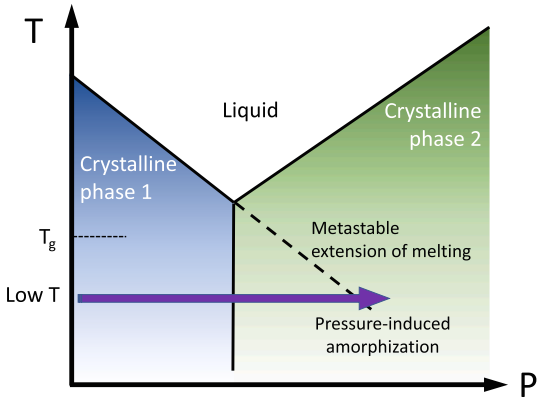


**Fig. 4.** Schematic description of pressure induced amorphization as a metastable melting event. At low pressure, phase 1 has a negative melting slope which ends on the stability field of the high-pressure phase 2. If compression is carried out at such a low temperature that transition to phase 2 is kinetically inhibited, the system can meet first the metastable extension of the melting curve of phase 1. Below the glass transition temperature, this will result in a solid-state amorphization. Modified from [86].

approached today by the configurational energy landscape concept [134] represented by the potential energy surface. The potential energy surface represents the potential energy of a given system as a function of all relevant atomic coordinates. It is generally a high-dimensional function but it is often represented in a more simplified way as a projection in a space of configurations (representing an arrangement of particular atoms). This allows, as in the Fig. 5, to put in relation one or more particular crystalline phases and "the" amorphous state. The relative potential energies of the local minima determine the equilibrium thermodynamic properties while the dynamics and kinetics depends upon how these minima are connected.

Each crystalline phase corresponds to a deep energy minimum. Depending on the thermodynamic conditions, this or that crystalline structure is more stable and a transition can operate by crossing a potential barrier. In addition to these deep minima, there is a complex landscape corresponding to amorphous states represented by shallow basins generally separated by low energy barriers. Under the influence of an external solicitation (the case discussed here is pressure, but the concept is much more general), the energy minimum of the starting phase (crystal 1 in Fig. 5) is increased in a significant way so that the energy barrier to amorphous states can be lower than that to another crystal phase (*e.g.* crystal 2).

## 4. The role of deviatoric stresses and shear instabilities

The experiments of amorphization under pressure of quartz showed a great dispersion of the transition pressures which spread in the range 10–30 GPa. This variability could be correlated to the degree of non-hydrostaticity due to the pressure transmitting medium in the diamond anvil cells [68]. The greater the deviation from hydrostaticity, the lower the amorphization pressure. Amorphization of $\alpha$-quartz can even be triggered under the shear stresses of a mortar grinding, *ca.* 0.4 GPa [159]. The influence of non-hydrostatic compression of $\alpha$-quartz has been investigated in MD simulations by Badro *et al.* [6] emphasizing the different response to compression along [0001] compared to other directions. Compression experiments in a diamond anvil cell without confining medium were conducted by Cordier *et al.* [28] on quartz and its structural analogue, $AlPO_4$ berlinite, which show the development of amorphous shear bands (Fig. 6a). Similar shear bands are observed in stishovite compressed under highly non-hydrostatic conditions (Fig. 6b). A spread of the amorphization pressures between 30 and 70 GPa was also observed for olivine and attributed to non-hydrostatic stresses [53,4,110]. In 2020, Kranjc *et al.* [72] reported development of amorphous shear bands in olivine micropillars compressed at room temperature under a uniaxial stress of 4 GPa.

In high-pressure experiments, non-hydrostaticity often develops during decompression. Yan *et al.* [143] report depressurization

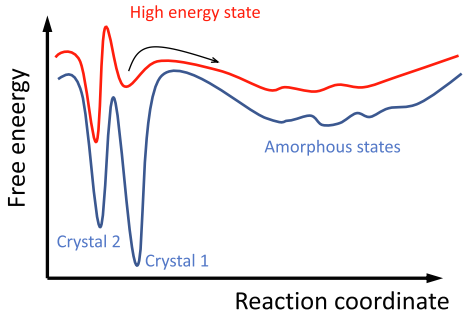


**Fig. 5.** Schematic configurational energy landscape diagram (after [87]) illustrating how the internal free energy of the system depends on the collective coordinates of all its atoms. In blue is the reference state with two crystalline phases, "1" being the most stable. In red is the system driven by some process (pressure, stress, defect content, irradiation, etc…), transition into an amorphous state is kinetically favorable.

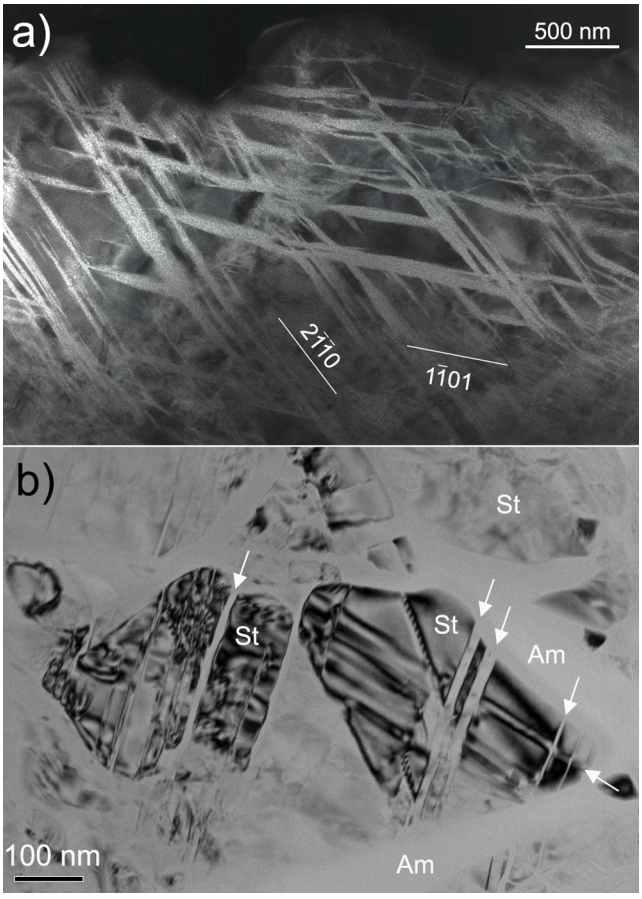


**Fig. 6.** Formation of amorphous shear lamellae under quasi-static high-pressure compression a) Quartz single crystal plate compressed at *ca.* 10 GPa in a diamond anvil cell without confining pressure medium. Transmission electron micrograph diffuse dark field (amorphous material appears brighter). b) Aluminum-bearing stishovite powder compressed without pressure-transmitting medium in a diamond anvil cell at *ca.* 40 GPa. Amorphized zones appear as wide veins (Am) and lamellae (arrowed). Transmission electron micrograph, bright-field. Sample: A. Rosa, S. Merkel, C. Sanchez-Valle.

amorphization of single-crystal boron carbide ($B_4C$) loaded to 50 GPa in a diamond anvil cell with stiff $B_4C$ powder used as the pressure-transmitting medium (or simply without pressure-transmitting medium). Amorphization was followed *in situ* by Raman spectroscopy. The characteristic bands of amorphous $B_4C$ did not appear until pressure was down *ca.* 15 GPa. In comparison, when the same experiment was repeated with soft NaCl as the pressure-transmitting medium, a specimen pressurized to 50 GPa was depressurized to 1.1 GPa without showing any sign of amorphization indicating that nonhydrostatic stresses play a critical role in this transformation.

Evidence of the importance of shear was also provided by shock experiments. Amorphization bands have been interpreted as localized melting on adiabatic shear bands by Grady [46,164]. Zhao *et al.* [149] present laser-shock results on four covalent solids, namely silicon (Si), germanium (Ge), boron carbide ($B_4C$) and silicon carbide (SiC). Transmission electron microscopy examination of the recovered samples shows amorphous band morphologies which suggest that shear stresses played a role in their formation. In SiC, both evidence for bands perpendicular to the shock direction and inclined along the maximum shear stress direction with a magnitude estimated at 25 GPa [148] are presented (Fig. 7).

Similar observations have been made on shock-loaded boron carbide exhibiting very narrow amorphous lamellae formed by localized mode II or mode III shear [23]. Further investigation using annular bright-field,

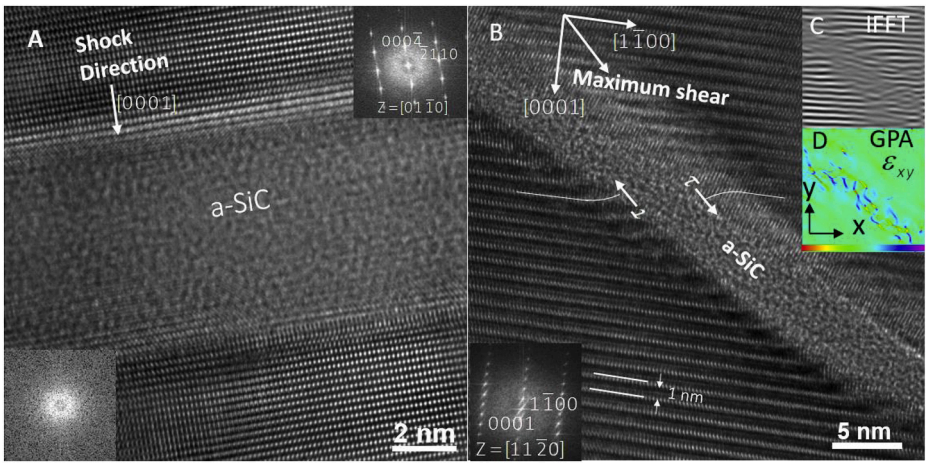


**Fig. 7.** HRTEM of recovered laser-shocked SiC. a) the amorphous band is perpendicular to the shock wave propagation direction. b) inclined amorphous band showing lattice distortion at the interface. c) Fourier filtered image of b). d) Geometric phase analysis showing the strain in the vicinity of the band. From [148] with permission.

aberration (Cs) corrected scanning transmission electron microscopy confirmed that the formation of these bands results from the disassembly of the icosahedra driven by shear stresses [107].

These observations suggest that amorphization is not only a response to pressure but may require the overall consideration of the mechanical stability of a crystal structure subjected to a complete stress tensor. The mechanical stability of crystals was studied by Born [14] who postulated that the loss of shear rigidity leads the transition to melting. In a further paper, Born [15] extended the analysis expressing that for a crystal to be stable, any deformation must increase the stored elastic energy. For a cubic crystal, the Born criteria is expressed by:

$$C_{11}+2C_{12}>0; C_{11}-C_{12}>0; C_{44}>0 \quad (1)$$

Where $C_{ij}$ are the elastic constants in Voigt notation. This approach also applies to lower-symmetry crystal classes [94]. The above conditions have simple meanings. The first one expresses stability against hydrostatic compression since $B=(C_{11}+2C_{12})/3$ is the isothermal Bulk modulus. The two other conditions express that the two shear moduli $G=C_{44}$ and $G^{'}=(C_{11}-C_{12})/2$ must have non-zero values. Under hydrostatic loading (pressure $P$), these relations transform into:

$$B=\frac{1}{3}(C_{11}+2C_{12}+P).>0; G^{'}=\frac{1}{2}(C_{11}-C_{12}-2P).>0; G=C_{44}-P>0 \quad (2)$$

It is important to emphasize that such criteria can only reveal the limits of stability of a structure without prejudging its evolution. Thus, Tang and Yip [132] show that, for SiC in the zinc blende structure, they account for the amorphization transition which is triggered by the vanishing of $G(P)=C_{44}-P$. In contrast, during hydrostatic compression of Si, the vanishing of $G^{'}=\frac{1}{2}(C_{11}-C_{12}-2P)$ has been interpreted by Mizushima *et al.* [93] as the cause of the transition from diamond cubic to the $\beta$-tin structure.

The Born criterion highlights the importance of shear instability in amorphization. In the form presented above, it only allows for hydrostatic loading. The sensitivity of the structure to non-hydrostatic loading can be assessed by calculations at the atomic scale. Karki *et al.* [165] used *ab initio* calculations to calculate the elastic stiffness tensor coefficients ($c_{ijkl}$) which provide a generalization of the zero-stress elastic constant tensor valid under arbitrary stress [7]:

$$c_{ijkl}=\left(\frac{\partial\sigma_{ij}(x)}{\partial e_{kl}}\right)x \quad (3)$$

Where $\sigma_{ij}$ and $e_{kl}$ are the applied stress and Eulerian strain tensors, and X and x are the coordinates before and after the deformation.

The elastic stiffness tensor coefficients ($c_{ijkl}$) are related to the zero-stress elastic constants ($C_{ijkl}$) by:

$$c_{ijkl}=C_{ijkl}+\frac{1}{2}\left(\delta_{ik}\sigma_{jl}+\delta_{jk}\sigma_{il}+\delta_{il}\sigma_{jk}+\delta_{jl}\sigma_{ik}-2\delta_{kl}\sigma_{ij}\right) \quad (4)$$

with $\delta_{ij}$ being the Kronecker delta symbol and $\sigma_{ij}$ being the applied stress tensor [136] (in [136] $c_{ijkl}$ is denoted $B_{ijkl}$).

Despite the general scope of this approach, Karki *et al.* [165] used it only to describe phase transitions in MgO and CaO (first-order B1-B2 transition), $SiO_2$ (second-order rutile to $CaCl_2$ transition) and Si (transition from diamond cubic to the $\beta$-tin structure). In all cases, they noted that the relevant generalized elastic stiffness coefficient associated with the relevant deformation softens toward the transition. They underline the analogy with the $B_{1g}$ mode in $SiO_2$ which softens, though not to zero, on approach to the transition. This shows that in that case, softening of phonon modes (see below) and of elastic stiffnesses give consistent indications. Atomic scale calculations are also a very efficient approach to directly evaluate the mechanical stability of solids under various loadings. First-principles or empirical potentials-based calculations are now commonly used to calculate the theoretical (or ideal) stress introduced by Frenkel in 1926 [40] and further linked to the mechanical stability by Hill [60]. The ideal stress is determined by straining the crystal in a series of incremental strains (of any kind: uniaxial tensile, simple shear, etc…) and calculating the fully relaxed energy and volume as a function of strain. The Cauchy stress is taken as the derivative of the free energy with respect to the strain [99,117,166]. The instability corresponds to the inflexion point in the free energy curve which corresponds to the maximum of stress (see an illustration on forsterite in Fig. 8).

The stability criteria (equations 1 or 2) can be regarded as the long wavelength limit of the general condition for vibrational stability of a lattice: *i.e.* the energy of all phonon modes must be positive. A phonon that would lower the energy of a crystal would grow in amplitude until the structure is driven to a new state [78,27]. Binggeli *et al.* [8] have calculated the phonon spectrum of quartz as a function of pressure. They show that the lowest acoustic branch of quartz softens with increasing pressure and becomes unstable when the oxygen atoms approach a nearly close-packed bcc arrangement. The role of non-hydrostatic stresses on phonon dispersion has been addressed by Choudhury and Chaplot [25]. They show a drastic change of phonon dispersion along the Γ-A direction for uniaxial compression along the *c*-axis, lowering the instability threshold. This behavior is not unique, coesite, like quartz, possesses a shear instability closely coupled to a zone-edge phonon softening at pressures comparable to the amorphization transformation [32].

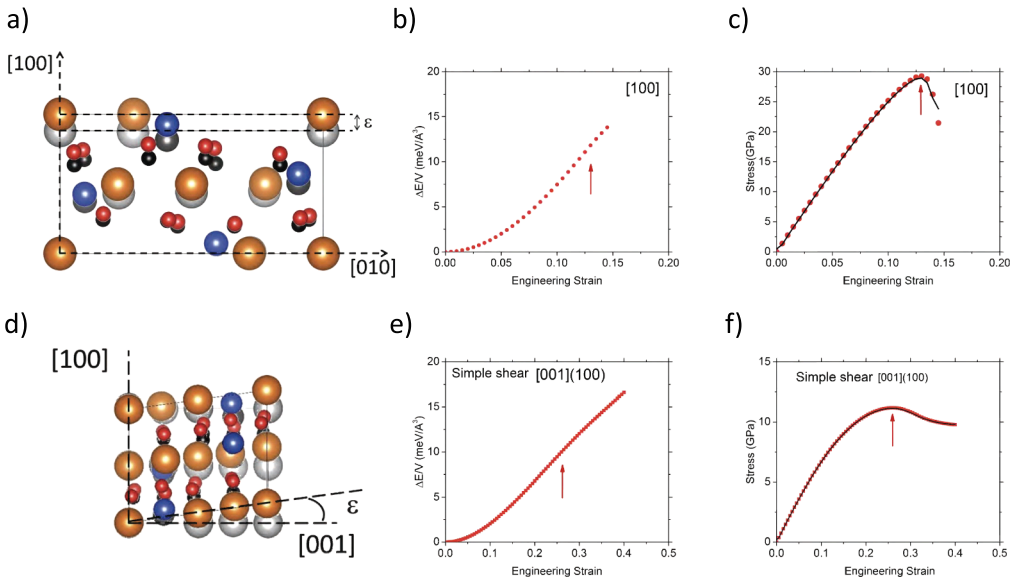


**Fig. 8.** Ultimate properties of forsterite $Mg_2SiO_4$. a, d) illustration of the loading conditions in tension along [100] in (a) and in simple shear along [001](100) in (d). b, e) Evolution of the strain energy as a function of the engineering strain in tension (b) and shear (e). c, f) Stress as a function of the engineering strain in tension (c) and shear (f). The lines correspond to the Cauchy stress from the derivative of the energy curves. The symbols are stresses directly provided by VASP. The instability is indicated by the red arrows in b, c, e and f. After Gouriet et al. [45].

## 5. The role of defects

The approaches to the mechanical instability of solids presented above only consider the case of the perfect crystal which is very rarely encountered. Real crystals usually contain defects which represent a beginning of disorganization of solids but also potentially sources of internal stress. They are therefore likely to play a role in amorphization. Considering again the analogy with melting, we can refer to the work of Poirier proposing a dislocation-based theory of melting [104]. Since dislocation locally break the long-range order, the assumption behind dislocation melting is to consider the melt as a crystal saturated with dislocations. Poirier and Price [105] also point out that the presence of dislocations dilates the lattice. This one being anharmonic, the dilation leads to a decrease of the shear modulus. We can therefore suppose that below the glass transition temperature, the accumulation of dislocations which lower the shear modulus and destroy the local order can cause amorphization. This mechanism has often been invoked in the case of ball mill-induced amorphization which often shows evidence of grain size reduction interpreted as the result of severe plastic deformation [18,125]. In single crystal $Ge_2Sb_2Te_5$ nanowire memory devices, Nam *et al.* [97] show direct evidence by transmission electron microscopy of amorphization resulting from dislocation jamming. Besides dislocations, the role of elastic distortions at disclinations has been discussed from a theoretical point of view, in particular for disclination quadrupoles in deformed nanomaterials [10].

Indentation which induces very localized deformations and builds under the indenter high confining pressures is a test conducive to amorphization. In 2009, Lin *et al.* [79] reported a characterization of indented $\gamma$-$Y_2Si_2O_7$ which is a refractory ceramic material. The similarities between the organization and properties of amorphous layers and those of slip bands led the authors to propose that amorphization is mediated by slip bands containing a high density of dislocations [79]. Two mechanisms are considered by the authors. The first one, which reminds the one of dislocation-melting, results from the intense distortions induced by the exceptional accumulation of dislocations. The other would result from a high supersaturation of point defects created either by the intersection or by the annihilation of dislocations. These two mechanisms can obviously work together. Similar conclusions have been reached after indentation of ceramics and semiconductors. In SiC, Szlufarska *et al.* [127] have studied by molecular dynamics the deformation and amorphization below the indentor. They conclude that the growth and dynamics of dislocation loops responsible for the load drops are responsible for the amorphization. In GaAs, Li *et al.* [76] observed amorphization under the indent in association with high concentrations of defects (dislocations, stacking faults, microtwins) suggesting a causal link between severe local plastic deformation and amorphization. Amorphization has also been observed in indented silicon [26,126] or after mechanical scratching [89]. In both cases, evidence of plasticity was observed, but the authors did not conclude that the amorphization resulted from plasticity (but rather from the transition to the $\beta$-tin phase). The opposite conclusion was reached by Huang *et al.* [62] on ball-milled silicon. They observe in HRTEM that the amorphization is nucleated inside the grains in association with crystal defects (twins, dislocations) which play the role of nucleation sites. Very nice observations were recently reported by He *et al.* [58] by HRTEM during *in situ* deformation of micropillars that shed new light on the processes by which amorphization results from plastic deformation of silicon under high stress. They observe that when the loading reaches 14 GPa, a localized band of plastic deformation develops by propagation of perfect dislocations on {111} planes. Within this band, a layer of a new phase with a diamond-hexagonal (*dh*) structure is formed. Further compression leads to the nucleation of dislocations dipoles in the *dh*-Si layer (Fig. 9). These dislocations are not mobile and lead by accumulation to the formation of amorphous nanodomains. During this process, the dislocation density increased from $3 \times 10^{16}$ m$^{-2}$ to $3 \times 10^{17}$ m$^{-2}$. The transition to the $\beta$-tin phase was not observed during this experiment. Chen *et al.* [24], in a numerical study (molecular dynamics) also on silicon, propose a slightly different mechanism. Considering the deformation of bicrystals, they induce 60° shuffle dislocation pile-ups that generate sufficiently large stress concentrations at the tip of the pile-up to trigger the formation of amorphous bands.

Grain boundaries can also play the role of nucleation sites for amorphization. Ovid'ko and Reizis [167] put the emphasis on the influence of elastic distortions induced by a grain boundary as those induced by grain boundary dislocations. The specific role of grain boundary structure and bonding at grain boundaries can be assessed by atomic scale calculations [100]. Kohyama *et al.* [70,71] performed *ab initio* tensile tests on SiC containing a {122} $\Sigma = 9$ tilt grain boundary showing a *ca.* 20% reduction in strength compared to the perfect crystal. Comparable calculations ({122} $\Sigma = 9$ tilt grain boundary) performed on aluminum led to the same conclusion [81]. However, in alumina, a $\Sigma 13[1\bar{2}10]$ pyramidal twin GB exhibits a strength reduction greater than 60 % [96] compared to perfect alumina [147].

The role of amorphization at grain boundaries is particularly expected in nanocrystalline materials where grain boundaries represent a significant fraction of the solid compared to the bulk. Indeed, severe

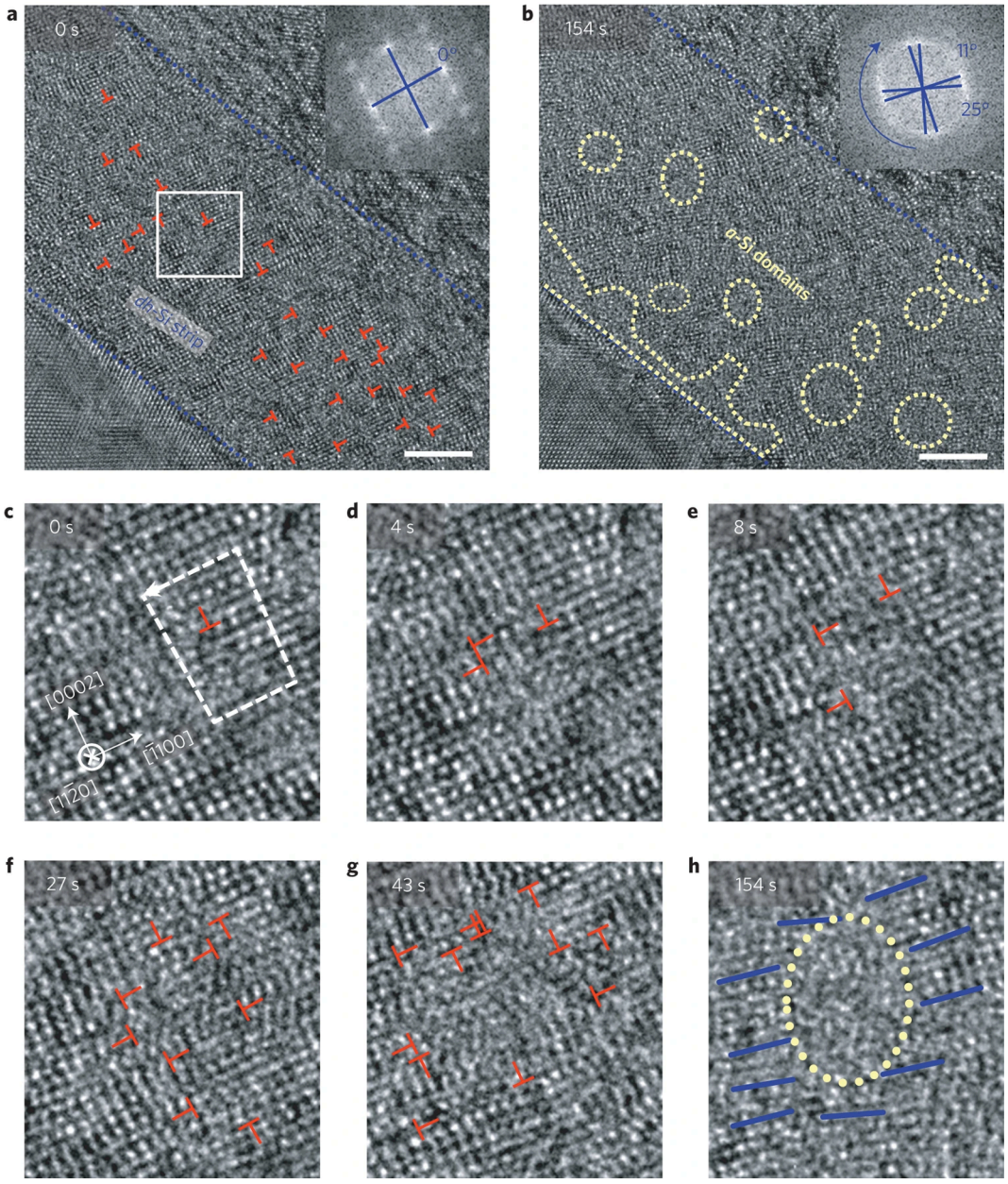


**Fig. 9.** Shear-driven amorphization in silicon a) HRTEM image of the *dh*-Si strip before formation of amorphous domains. b) HRTEM image showing formation of nanosized amorphous domains (marked by dotted circles). Scale bars in a,b, 5 nm. Insets (a,b): fast Fourier transform of the strip, with blue crosses tracking the rotation of the *dh*-Si lattice, and the *dh*-Si lattice in the strip pulverized and rotated during the shear-driven amorphization process. c–h) Time-lapse HRTEM images of the boxed region in a, showing the atomic-scale process of formation of an amorphous domain via dislocation accumulation. Dashed lines and arrow in c indicate the Burgers circuit and Burgers vector, respectively. The blue lines in h mark the individual basal planes around the amorphous domain (indicated by a dotted circle). He *et al.* [58] with permission.

plastic deformation (SPD) processes intended to induce grain size refinement sometimes lead to amorphization. In 2004, Huang *et al.* [63] reported evidence by HRTEM of preferential amorphization at grain boundaries (and dislocations) in TiNi, a B2 intermetallic compound processed by high-pressure torsion (HPT) at 5 GPa. The grain size before amorphization was 10 nm which led the authors to estimate the energy stored at grain boundaries to 2.2 kJ.mol$^{-1}$. This value is comparable to the energy stored by dislocations (estimated to 2 kJ.mol$^{-1}$ for a dislocation density of the order of $10^{17}$-$10^{18}$ m$^{-2}$). Yamada and Koch [141] already observed a grain size of 5 nm in TiNi before amorphization by ball milling. They estimated the grain boundary energy to about 4.11 kJ.mol$^{-1}$ and, after comparison of this value to the enthalpy of crystallization measured by differential scanning calorimetry (3.15 kJ.mol$^{-1}$), they concluded that energy stored at grain boundaries was driving amorphization. Following Yamada and Koch, Huang *et al.* [63] concluded that dislocations and grain boundaries provide the driving force for amorphization in HPT-processed TiNi. In a later study on TiNi deformed by HPT, Peterlechner *et al.* [103] note that ultrathin amorphous ribbons first form at grain boundaries which are intersected by shear bands which develop in a second stage. Twin represent a special kind of boundaries with, in principle, a much lower energy than normal grain boundaries. Quantum mechanics calculations by An *et al.* [3] suggest that, in $B_6O$, amorphous bands nucleate preferentially at the twin boundaries because the twinned structure has a lower maximum shear strength by 7.5 % compared with perfect structure. They find however that once nucleated, the amorphous bands extend

preferentially along $\{\bar{1}012\}$ planes (which does not coincide with the twin boundary planes), possibly due to the complex stress conditions in their nanoindentation experiments. Grain boundary amorphization seems to be rather common in superhard ceramics and has also been reported in indented nanocrystalline boron carbide, $B_4C$ [52]. To interpret this behavior, Yang *et al.* [144] performed DFT calculations on systems containing grain boundaries along (111). Under pure shear deformation, the ideal strengths of these systems are 35–39 % lower than perfect $B_4C$. They also showed that Fe-doping of the boundaries leads to a further strength reduction.

Demkowicz *et al.* [36] report a numerical study where a quasi-columnar nanocrystalline (8 nm) Si structure containing pure tilt boundaries was deformed at 300 K. During deformation, the intra-granular regions are characterized as liquid-like amorphous silicon (following a distinction made by Demkowicz and Argon [34–35] between different atomic environments: 'liquid-like' and 'solid-like' in amorphous silicon).

Very recently, grain boundary amorphization was reported by Samae *et al.* [109] in olivine aggregates (average grain size 2.8 μm) deformed at 900–1200 °C, 300 MPa [41], and in coarser aggregates (grain size 20–100 μm) deformed at 1000–1200 °C, 5 GPa [12]. In these specimens, amorphization was also observed at boundaries between olivine and pyroxene grains, however the amorphous layer has the olivine composition [109]. Amorphization has previously been reported at phase boundaries in Cu/Nb nanocomposite wires [111]. Molecular dynamics modeling of this process shows that amorphization depends on the interface. Zhou *et al.* [152] show that interface with Nishiyama–Wassermann (NW) orientation relationship or interfaces with Kurdjumov–Sachs (KS) orientation relationship with a {111}fcc||{110}bcc habit plane consistently deform via pure interface sliding. In comparison, at 100 K, interfaces with KS orientation relationship and with a {112}fcc||{112}bcc habit plane amorphize. The amorphous layer then grows as the square root of stain $\gamma^{0.5}$. The magnitude of shear strength differs with the orientation relationship, the shear resistance being smaller for interfaces that do not amorphize. The formation of amorphous layers of the {112}KS interface at large strains depends on the temperature. Between 400 and 600 K, amorphization takes place, but the strain exponent decreases to 0.44 at 400 K and 0.26 at 600 K. above 800 K amorphization is not observed. An interesting observation is that the {112}KS interface keeps a stable strength from $\gamma = 3-4$ to $\gamma = 40$. The shear strength of {112}KS does, however, vary with temperature. It decreases from 1.87 GPa at 100 K to 1.29 GPa from 800 K to 1000 K.

## 6. Amorphization as a deformation mechanism

a) Deformation under shock loading

The difficulty in monitoring shock experiments as deformation tests led first to consider the influence of shock on the mechanical properties. In case of boron carbide ($B_4C$) a drop of shear strength was observed when the stress exceeded the Hugoniot elastic limit (Fig. 10a), retaining only a fraction of that in the elastic regime [133]. This drop can be attributed to the development of thin amorphous bands (Fig. 10b, [23].

Dynamic indentations (indentation-induced strain rate 1000 $s^{-1}$) performed on fine-grained (*ca.* 2 μm) boron carbide also resulted in a decrease in hardness and fracture toughness which was interpreted as a consequence of the formation of a localized amorphous phase detected by Raman spectroscopy [43]. The influence of amorphization on toughness has been little studied since most studies involve high confining pressures. However, Subhash *et al.* [124] show that under the indenter, cracks can nucleate along the amorphous lamellae (Fig. 11) and propagate to regions of lower pressure (the pressure field is very heterogeneous under the indenter). This is reminiscent of the fracturing of amorphized grain boundaries observed by Gasc *et al.* [41] in olivine aggregates deformed below 1000 °C (see Fig. 15b below). Amorphization can therefore under certain circumstances constitute a failure mechanism.

Shock compression by short duration pulsed laser of SiC reported by Zhao *et al.* [149] involves a peak shock pressure of 50 GPa and an associated shear stress of 25 GPa. The temperature history of the test is not indicated. Observation of recovered samples and molecular dynamic simulations indicate that the response of the material is a combination of coupled hydrostatic compression and shear. The volumetric strain results from the amorphous phase being 6.4 % denser than the crystal. The shear strain was not measured.

In 2009, Gutkin and Ovid'ko [51] proposed a first micromechanical

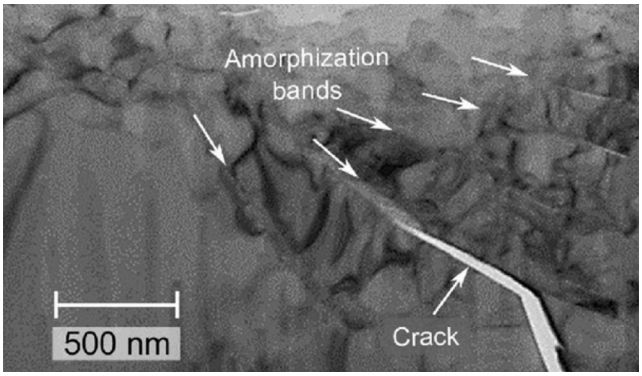


**Fig. 11.** Transmission electron microscopy showing amorphization bands and a crack beneath indentation on a boron carbide ($B_4C$) sample. Modified after Subhash *et al.* [124] with permission.

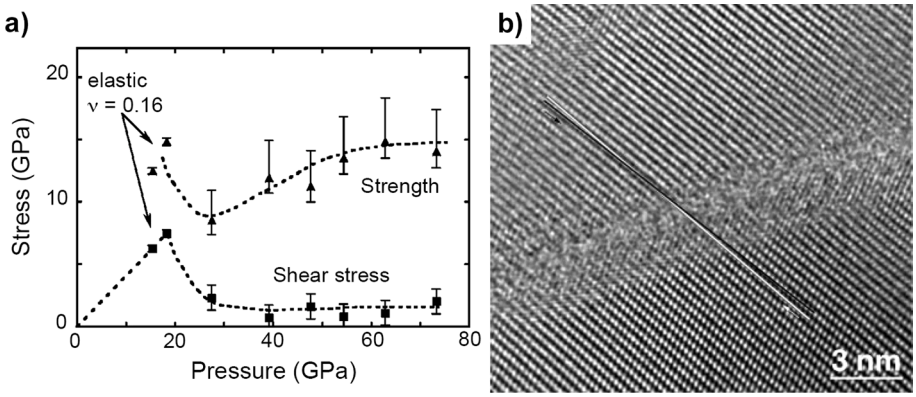


**Fig. 10.** Shock-induced amorphization of $B_4C$. a) Shear stress and strength of $B_4C$ in the shocked state estimated from reshock and release experiments. After Vogler *et al.* [133] b) TEM observation of a fragment of $B_4C$ produced by a ballistic test at a hypercritical impact velocity of 907 m/s (23.3 GPa). Misalignment of the lattice fringes on either side of the amorphous zone is highlighted by the lines and was measured to be 1°, indicating shear. After [23] with permission.

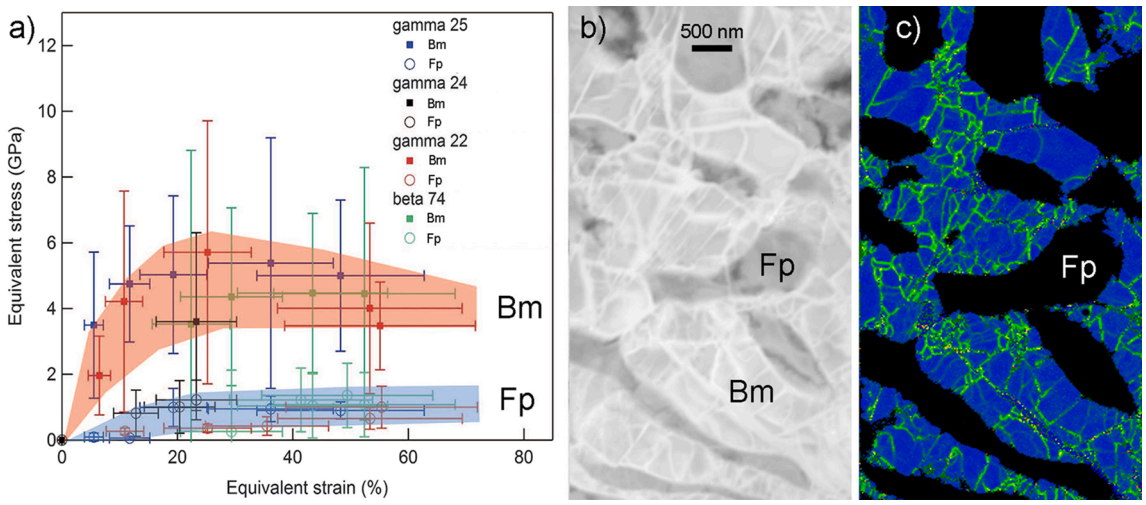


**Fig. 12.** Stress-induced amorphization in bridgmanite at high-pressure, high-temperature. a) Equivalent stress in bridgmanite (Bm) and ferropericlase (Fp) as a function of strain. Deformation conditions are 2150 K, 27.5 GPa for gamma 25 and gamma 24; 2130 K, 27 GPa for gamma 22; 2000 K, 24.1 GPa for beta 74. Modified from Girard *et al.* [44] with permission. b) Sample gamma 21 (2130 K, 27 GPa) from Girard *et al.* [44]. Scanning precession electron diffraction virtual bright field where the amorphous lamellae in bridgmanite appear brighter than the crystalline parts (ferropericlase appear even darker). c) Kernel Average Misorientation (KAM—third neighbor) from b) in bridgmanite (ferropericlase not considered here appears in black). This representation highlights local gradients of orientation (in green). One can see that amorphous lamellae correlate with high KAM, demonstrating that they localize shear.

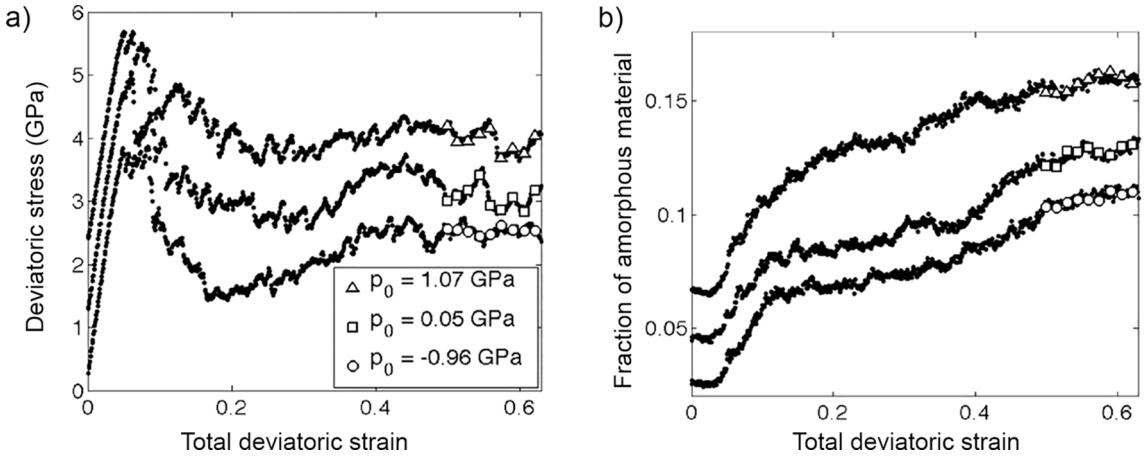


**Fig. 13.** Nanocrystalline silicon a) deviatoric stress versus strain during plain strain numerical plastic deformation of a nanocrystalline Si polycrystal at 300 K, 2.58 × $10^8$ $s^{-1}$. $p_0$ corresponds to three levels of applied initial dilatations. The curves have been offset by increments of 1 GPa for clarity. b) Evolution of the fraction of amorphous material as a function of strain corresponding to the 3 tests represented in a). The curves have been offset by increments of 0.02 for clarity. After Demkowicz *et al.* [36].

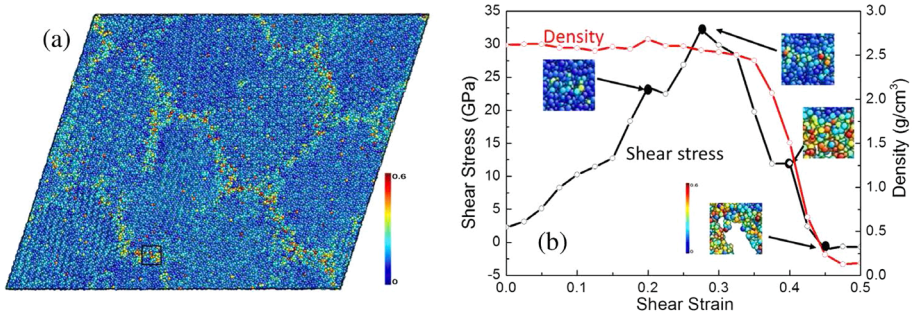


**Fig. 14.** Nanocrystalline Boron Carbide a) snapshot of a $B_4C$ nano-aggregate at 0.325 shear strain. b) (b) Local hear-stress – shear-strain and density-shear-strain relations from a 1 nm × 1 nm × 1 nm triple junction region (dark square in (a)). Some snapshots of critical states are extracted. Atoms are color coded based on the atomic shear strain. Guo *et al.* [52] with permission.

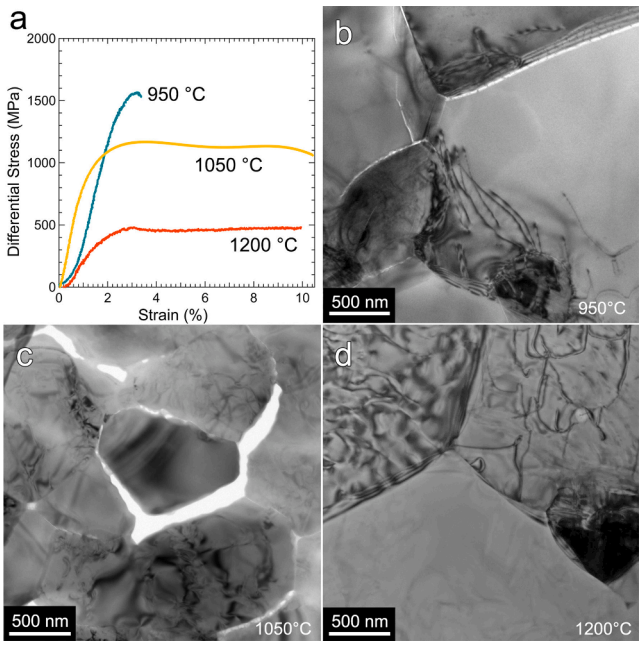


**Fig. 15.** Axial compression of olivine aggregates in a Paterson press (300 MPa confining pressure), Gasc *et al.* [41] a) mechanical data. b) Evidence of brittle failure of amorphized grain boundaries at 950 °C. c) grain boundary sliding and grain boundary ductile deformation at 1050 °C d) at 1200 °C evidence are mostly intracrystalline plasticity by dislocations. b, c and d: bright-field transmission electron micrographs.

model to describe plastic flow in a solid undergoing amorphization. In this model, shear localizes in oblate ellipsoidal nuclei oriented along the maximum resolved shear stress, or at grain boundaries. Formation and growth of the nuclei is studied from the energetic point of view highlighting a shear stress threshold for the process becoming energetically favorable. Zeng *et al.* [145,146] developed a multi-mechanism constitutive model to describe plastic deformation and failure of a quasi-brittle solid undergoing amorphization. They suppose that, above a given threshold stress, amorphization occurs along multiple sets of parallel bands controlled primarily by the local stress state (rather than crystallography). Both the pressure and the shear stress contribute to the onset of amorphization. Densification within the shear introduces a normal deformation as well as a coupled shear deformation. After formation of the bands, subsequent flow of the amorphous materials in the bands is described with a Bingham viscoplastic model. To account for failure, the authors assume that the shear resistance decreases with increasing shear deformation and that damage occurs at the intersection of sliding bands. When damage reaches some critical threshold, granular flow is activated. This model can account for the drop of shear strength described by Vogler *et al.* [133] (Fig. 10a). The authors underline the fact that the quality of the model depends on the knowledge of the material parameters which is incomplete.

b) Deformation under quasi-static high-pressure compression

In quasi-static high-pressure research, megabar pressures are reached by compressing thin specimens in diamond anvil cells. In most cases, efforts are made to make the experiments as hydrostatic as possible. However, the complete removal of deviatoric stresses is very difficult, if not impossible when the confining medium becomes solid. In some experiments, the non-hydrostaticity is exploited to provide information on the rheology of solids under high pressure. Compression can thus be accompanied by large plastic deformation of the sample. In this case, the *in situ* stress or even the development of textures is measured from X-ray diffraction data [84,137]. Several examples have been provided above that show that plastic deformation in diamond anvil cell can be accommodated by amorphization, either intentionally (*e.g.* [28,143]) or not. An unwanted and undetected contribution of amorphization might be the origin of controversies about deformation mechanisms activated at high-pressure when crystal preferred orientations are interpreted as the result of dislocation glide only (see for instance the conflicting results on post-perovskite [92]).

At lower pressure (below *ca.* 25 GPa) deformation experiments are now routinely performed using multianvil apparatuses [30,142,135]. In 2016, Girard *et al.* [44] performed the first deformation experiment of an assemblage representative of the mineralogy of the lower mantle (*i.e.* at depths greater than 670 km) under representative (P,T) conditions. This assemblage is composed of (Mg, Fe)O ferropericlase ( 20 %) and (Mg, Fe) $SiO_3$ bridgmanite, a silicate with a perovskite structure. The sample was deformed under 27 GPa and 2130 K, by torsion in a rotational Drickamer apparatus [142] at a strain rate of $3 \times 10^{-5}$ $s^{-1}$. The maximum strain estimated from the angle of rotation of the anvil reached 100 %. Stress was measured from X-ray diffraction at the synchrotron X-ray radiation facility (Fig. 12). The stress partitioning between ferropericlase and bridgmanite is reproduced Fig. 12a. Under these conditions, bridgmanite appears substantially stronger than ferropericlase. The deformation microstructure of a recovered specimen was investigated by TEM by Nzogang *et al.* [98]. The ferropericlase grains are crystalline, very elongated and contain a large density of dislocations. In contrast, coarse-grained (several micrometers) bridgmanite shows only pervasive amorphous deformation lamellae. Their contribution to *in situ* deformation was attested by misorientation measurements across the lamellae (Fig. 12c). Shear amorphization was thus the only deformation mechanism active in bridgmanite under these conditions. It is remarkable that despite the high temperature (2130 K), amorphization occurred and that the aggregate dominated from a volumetric point of view by the bridgmanite has kept this exceptional strength (*ca.* 4 GPa).

Due to the high pressures created under the indentor (and the associated non-hydrostatic stresses), indentation tests have produced numerous evidences of amorphization. The most common parameter derived from indentation test is hardness which measures the resistance to local permanent deformation (penetration) of a material in response to activated deformation mechanisms. However, other mechanisms such as phase transformation can affect hardness. Amorphization, which exhibits both the characteristics of a phase transformation (through the associated volume change) and a plasticity mechanism (through the development of shear bands), is therefore likely to affect hardness measurements [124]). In the case of nanoindentation, the normal force *vs.* penetration curve is measured quasi-statically and dynamically (harmonic loading) allowing the hardness and modulus of elasticity of the material to be determined. Discontinuities in the nanoindentation load–displacement curves, referred to as a pop-in, are widely used to inform about activated mechanisms. Reddy *et al.* [106] show that load–displacement curves obtained from nanoindentation of single-crystal $B_4C$ show pop-in which can be linked to the onset of amorphous shear bands. A similar conclusion had been proposed in 2017 by Han *et al.* [54] from a large-scale molecular dynamics simulation of spherical nanoindentation on a (100) oriented Si single crystal.

c) Nanocrystalline materials and grain boundary sliding

Reduction in grain size generally leads to strengthening (the Hall-Petch effect). However, the development of nanocrystalline materials has revealed an inverse effect when the usual plasticity mechanisms (dislocations) give way to grain boundary sliding for small grain sizes [113]. Szlufarska *et al.* [128] have used molecular dynamics to simulate indentation at 300 K of nanocrystalline (average grain size 8 nm) SiC. "Macroscopic" yielding coincides with amorphization of grain boundaries which then yield plastically. Chavoshi *et al.* [21] also used molecular dynamics to study shear deformation of nanocrystalline silicon carbide ceramics as a function of grain size. They find a well-defined maximum in the shear strength for grain sizes in the range 6.2 to 7.7 nm. They also show that the shear modulus uniformly decreases as the grain size is reduced from 18.6 to 3.7 nm, demonstrating that the elastic properties of nanocrystalline SiC are directly correlated with the

fractions of amorphous grain boundary regions.

In their numerical simulation, Demkowicz *et al.* [36] have deformed a nanocrystalline (8 nm) Si quasi-columnar polycrystal containing 6 grains. Strain was applied at 300 K up to 117 % at a strain-rate of $2.58 \times 10^8$ $s^{-1}$. The stress–strain curves (Fig. 13) exhibit an initial high deviatoric stress followed by strain softening which corresponds to the onset and development of amorphous material at grain boundaries. Plastic deformation localizes exclusively at grain boundaries. Incompatibilities are accommodated by grain rotation, creation of new grains or eventually by nano-scale voids or cracks formation.

Nanocrystalline boron carbide $B_4C$ also exhibits a reverse Hall-Petch effect due to grain boundary sliding for grain sizes below 5 nm. Reactive molecular dynamics simulations show that the elastic regime is followed by a regime dominated by grain-boundary sliding which leads rapidly to amorphization of the grain boundaries. The onset of amorphization occurs in response of very high local stresses (*ca.* 32 GPa in case of the example presented in Fig. 14). Amorphization of the grain boundary leads to a sharp drop of the shear stress, probably linked to an acceleration of the local strain-rate. This might be the cause for the cavitation which initiates in the grain boundary soon after amorphization.

Although most studies of amorphization-driven grain boundary sliding deal with nanocrystalline materials, evidence exist that coarser-grained materials might be concerned. Gasc *et al.* [41] report deformation experiments at 950–1200 °C, 300 MPa of olivine aggregates with average grain size 2.8 μm. At 950 °C, the behavior is essentially brittle. Fig. 15b shows that failure occurs mostly at grain boundaries. Some dislocation accommodation can be seen. Further investigations [109] showed that these grain boundaries were amorphized. At 1050 °C, a ductile behavior is observed with very large displacements (in shear but also with tensile components) at grain boundaries which exhibit large amounts of amorphous material. At 1200 °C, it is only with HRTEM that amorphous materials can be revealed in some grain boundaries. Ductile behavior results mostly from dislocation creep. These experiments highlight the influence of the rheological properties of glass, and in particular the crucial role of the glass transition temperature on the mechanical properties of the aggregate. At 950 °C, the stress is very high (greater than 1.5 GPa), enough to amorphize the grain boundaries. At this temperature amorphous olivine is in the glassy state, below the glass transition temperature, and behaves in a brittle manner given the low confining pressure applied (300 MPa). At 1050 °C, the glass approaches or exceeds the glass transition temperature. The viscosity is lower and very important relative displacements between the grains are generated (leading to cavitation). Comparable experiments, but under a higher confining pressure (5 GPa) have been performed by Bollinger *et al.* [12]. The high confining pressure promotes grain boundaries deformation and inhibits fracture and cavitation (Fig. 16). Unfortunately, in this experiment mechanical data (stress versus strain) are not available.

The role played by an amorphized grain boundaries is not limited to the shear produced by sliding. Pan and Rupert [102] have shown that amorphous intergranular films help to accommodate repeated absorption of dislocations from intracrystalline plasticity as compared to ordered grain boundaries (Fig. 17). Crack nucleation is delayed and ductility is increased. Schuler *et al.* [112] also suggest that amorphous intergranular films might lower grain boundary energy and therefore limit grain growth.

In contrast to the previous cases, it may be grain boundary sliding that triggers the formation of amorphous intracrystalline shear bands. Luo *et al.* [82] present a numerical study (molecular dynamics with the EAM potential) of the plasticity of $SmCo_5$, an intermetallic with hexagonal structure. It is important to note that in this material, dislocation glide is quite difficult, suggesting an essentially brittle behavior. Samples with grain size ranging from 5 to 65 μm in diameter are loaded in uniaxial tension or compression at a strain rate of $10^8$ $s^{-1}$. Grain size softening is observed for grain sizes below 37 nm.

The primary activated deformation mechanism is grain boundary sliding. The authors do not report evidence for grain boundary amorphization. For grain size larger than 15 nm, grain boundary sliding builds stress concentrations in the vicinity of triple junctions as shown on Fig. 18. These stresses are relaxed by the nucleation of amorphous shear bands (Fig. 18c) which allow grain boundary sliding to proceed further accompanied by a sudden softening before the stress is stabilized. Further intracrystalline deformation also results from the nucleation of non-crystallographic shear bands which are the primary driver of plasticity in those samples.

d) Small scale samples

Recently, evidences have been provided of amorphous shear bands-based deformation after micropillar compression. Kranjc *et al.* [72] compressed single crystal olivine with (100) and (010) planes oriented at 45° of the compression axis at room temperature. Micropillars with diameter of 1.25 μm were used. Most pillars failed in a brittle manner. Some specimens show stable shear band deformation under a compressive stress of 4 GPa. A cross-section was examined by TEM showing no dislocation activity but thin amorphous shear bands in (100) planes. The strains produced are 5.8 % at $4 \times 10^{-6}$ $s^{-1}$, 1.4 % at $1 \times 10^{-6}$ $s^{-1}$ and 0.6 % at $5 \times 10^{-7}$ $s^{-1}$. The differences probably come from differences in the amount of amorphous shear bands activated.

Fig. 19 shows a micropillar of $SmCo_5$ deformed in compression by Luo *et al.* [83]. The pillars (8 μm long) are tapered (diameter 1.5 μm on

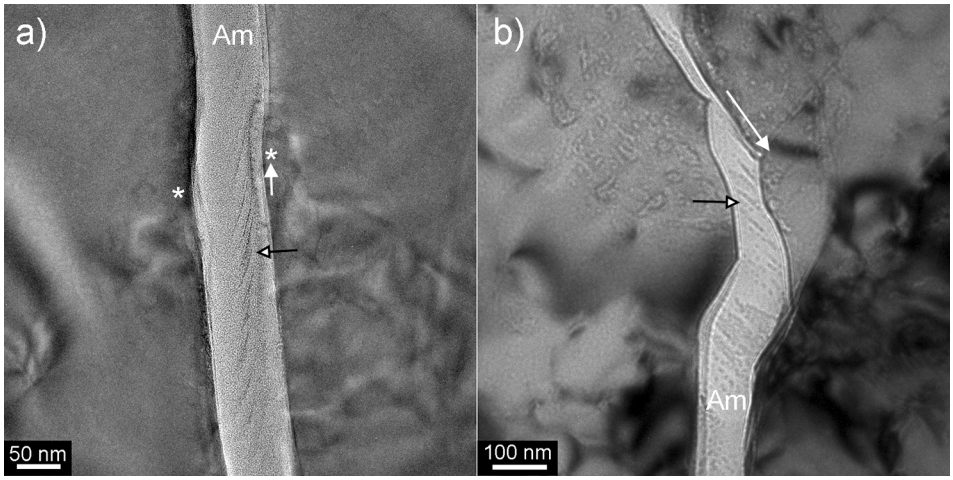


**Fig. 16.** TEM micrographs of olivine specimens deformed at 1000 °C, 5 GPa in a multianvil apparatus (Specimen references: a) M582, b) M640, see Bollinger *et al.* [12]). Evidence for shear are inferred from displacements of the crystal/amorphous boundaries (white arrows) and by the internal shear bands seen in this defocused mode (black arrows).

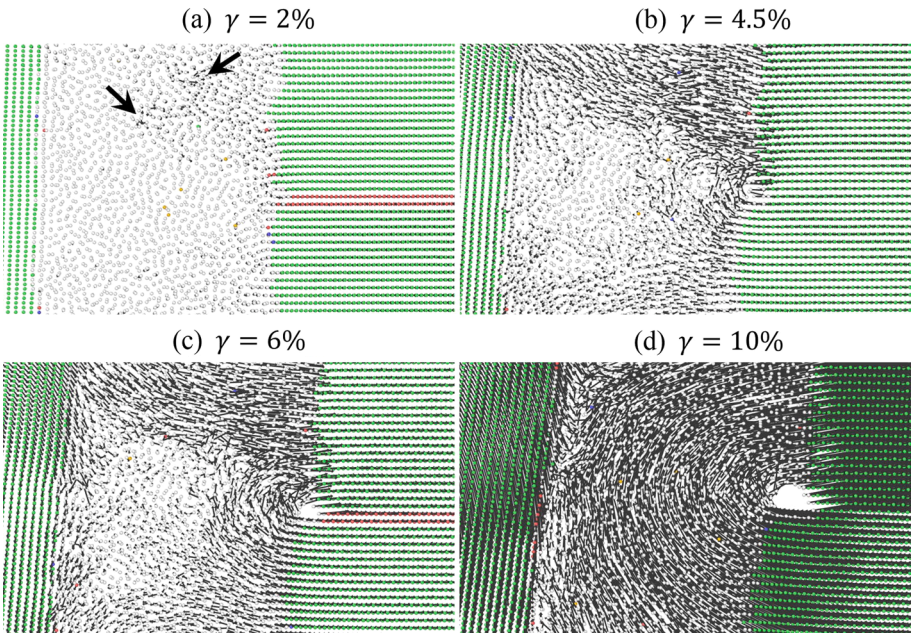


**Fig. 17.** Influence of amorphous intergranular films on toughening. Displacement field within a sample of Cu-Zr with a 5.7 nm thick amorphous intergranular film, loaded at a shear strain rate of $10^8$ $s^{-1}$, at applied shear strains of (a) 2% where the first leading partial dislocation is absorbed (red), (b) 4.5% where atoms in the amorphous layer move to accommodate the shift of the upper middle grain to the right, (c) 6% with a vortex flow which expands with increasing shear strain and number of absorbed dislocations, and (d) 10% with a crack nucleating at the amorphous crystal interface. Atoms are colored according to common neighbor analysis (green is fcc and red is hcp). The magnitude and direction of the displacement of each atom is indicated by the length and direction of the associated arrow. The two black arrows in (a) show the positions of two shear transformation zones. From [102] with permission.

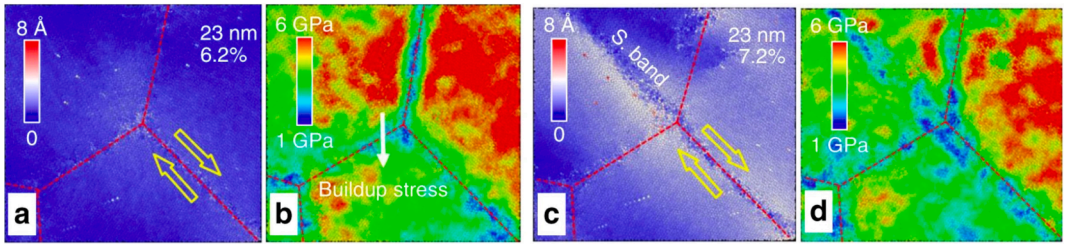


**Fig. 18.** Molecular dynamics simulation of $SmCo_5$ deformed at a strain rate of $10^8$ $s^{-1}$. Grain boundary sliding is highlighted by the yellow arrows. Displacements of atoms relative to their positions in the unstrained samples and distribution of von Mises stress in the same area around a triple junction for grain size of 23 nm under the strain of 6.2% (a, b), and the strain of 7.2% (c, d), respectively. The amorphous shear band seen in (c) relaxes the stresses built up by the grain boundary sliding (b). From Luo *et al.* [82] with permission.

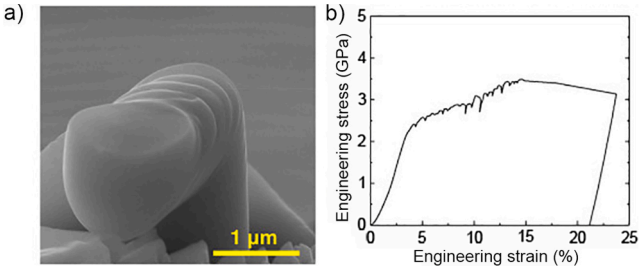


**Fig. 19.** Plastic deformation of $SmCo_5$ micropillars a) SEM micrograph of a $SmCo_5$ micropillar deformed by compression. b) Engineering stress–strain curve from an experimental micro-pillar compression. (after [83]).

top and 2 µm at the bottom) and prepared in a polycrystalline material with grain sizes in the micrometer range. The engineering stress–strain curve shows large plastic deformation up to 22 % engineering strain. This deformation results from single slip on a few localized shear bands which are supposed to be amorphous (no TEM observation is reported on these samples). The presence of amorphous shear bands and their major contribution to plastic strain was attested after indentation and by molecular dynamics simulations. Since these experiments were performed without confining pressure, deformation by amorphous shear bands shows not only that this mechanism prevails over dislocation plasticity, but also over fracture. The authors show that the energy of formation of the amorphous bands is lower than the cleavage energy.

Ovid'ko [101] suggested that amorphization is a specific deformation mechanism of single crystal nanowires through development of spatially inhomogeneous plastic shear along several neighboring planes. Ikeda *et al.* [65] used molecular dynamics to investigate the mechanical behavior of metallic nanowires (single crystals Ni and NiCu alloys) of section 2 nm × 2 nm. Strain rates between $5 \times 10^8$ $s^{-1}$ and $5 \times 10^{10}$ $s^{-1}$ were applied at 300 K. Up to $5 \times 10^9$ $s^{-1}$, the nanowire deforms by shear bands and twins, but remains crystalline (Fig. 20a). At $5 \times 10^{10}$ $s^{-1}$ the behavior is very different with amorphization taking place progressively from 7.5 % strain. At 15 % strain, the maximum stress (9.5 GPa) is reached and then decreases to reach a plateau at 3 GPa and 35 % strain where the nanowire flows with a viscosity of 0.06 Pa.s. Branicio and Rino [16] performed similar calculations varying the cross sections to evaluate surface effects which influence the elastic properties, but not the elastic limit (9.5 GPa at 10.5 % strain). In their experiments, amorphization was only observed for strain rates $\geq 7 \times 10^{10}$ $s^{-1}$ (Fig. 20b). The viscosity exhibited by the amorphous Ni (0.03–0.06 Pa.s) compares also very well with the one found by Ikeda *et al.* [65]. In both cases, amorphization leads to an increase of ductility.

Large strain amorphization-accommodated plasticity was reported by Han *et al.* [55]. SiC nanowires were bent *in situ* in a TEM at a strain rate of $10^{-4}$ $-10^{-5}$ $s^{-1}$. A clear amorphization is observed where strain localizes at the bending region with more amorphous material produced in the tensile region (Fig. 21). Due to the geometry, strain and stress could not be quantified. HRTEM of the deformed region shows tiny

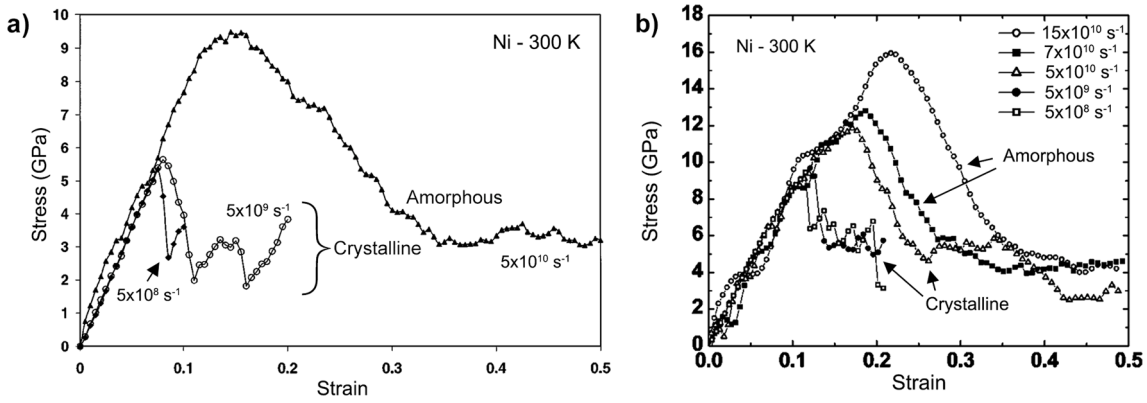


**Fig. 20.** Deformation of 2 nm × 2 nm Ni nanowires at 300 K – Strain rates are indicated in the figure. a) results from Ikeda *et al.* [65]. b) results from Branicio and Rino [16].

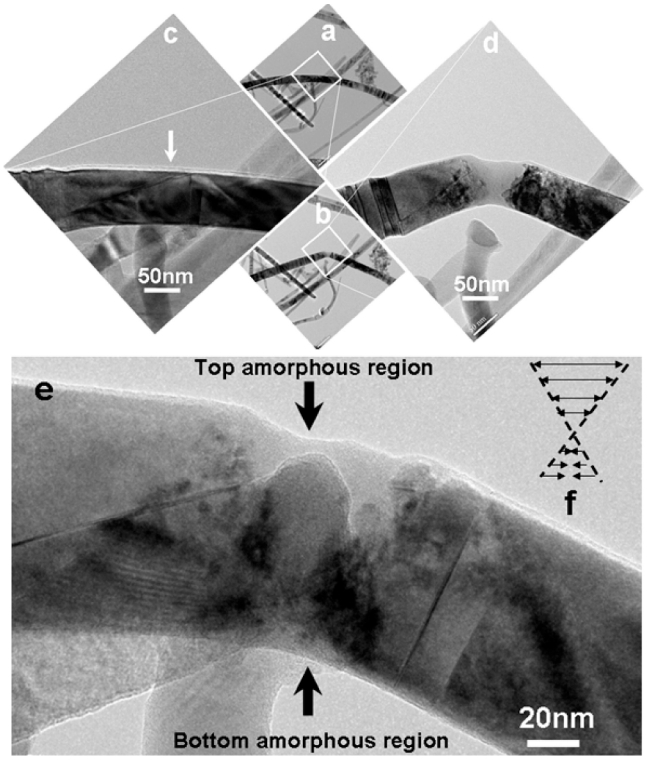


**Fig. 21.** SiC nanowire bent *in situ* in a TEM. a, b) before and after deformation with enlargements in c and d. e) enlargement showing the deformation-induced amorphous zone with a butterfly shape due to the compressive/tensile regions depicted in f). Reprinted (adapted) with permission from [55]. Copyright 2007 American Chemical Society.

remnants crystalline units in the amorphous matrix.

Tochigi *et al.* [130] have performed compression of quartz single-crystal nanopillars *in situ* in a transmission electron microscope. In one occurrence, the pillar adhered on the flat punch as a result of the compression test, so the pillar was elongated during the pull back. During this phase, the pillar underwent a very significant elongation estimated at 21 % (Fig. 22). The authors rule out a possible influence of a temperature rise (of the order of $10^{-6}$ K only), but recall that the experiment is carried out *in situ* with an electron beam current density of $1 \times 10^{7}$ pA.cm$^{-2}$. The effect of electron irradiation can be twofold. Quartz is known to be electron beam-sensitive and the amorphization may have been assisted by the irradiation. In addition, the deformation of amorphous silica is assisted by electron irradiation [151]. The observed high ductility of the pillar is probably influenced by this parameter.

## 7. Concluding remarks, open questions and perspectives

In this paper we have reviewed the evidence of amorphization as a result of a mechanical loading. Although it is not always measured, or even highlighted, this transformation is always accompanied by a strain, whether volumetric or shear. Many studies show that this instability is sensitive to shear, leading to the formation of amorphous shear bands. Ovid'ko [101] distinguishes two distinct categories of basic mechanisms. The first one considers amorphization as an ultimate stage of plasticity. This hypothesis was put forward very early in the case of ball milling [69] and more recently by Zhao *et al.* [150] in the case of high-entropy alloys. We have presented several studies that support this mechanism. The fundamental point is that it assumes that the material is plastic and that defects are produced. However, for various reasons, these defects are not mobile enough and accumulate (in a context that is certainly very hardening). There are several explanatory schemes to describe what happens next. According to Fig. 5, the local energy exceeds that of the amorphous phase. One can also evoke the role of local stress concentrations to trigger a static or dynamic instability.

The second mechanism does not consider traditional plasticity (resulting from defect propagation) as a prerequisite, but as a competing process. In other words, it is only when the usual plasticity mechanisms are inhibited that the stress will reach an instability threshold leading to amorphization. The inhibiting factors can be very diverse such as:

- purely hydrostatic compression
- very high strain-rates (shocks)
- very low temperatures
- materials with very high lattice friction
- very small sample sizes

It appears that these two distinct categories of basic mechanisms have been reported which shows that stress-induced amorphization is a phenomenon that can affect a wide range of materials. Once the instability has passed (in either scenario), the amorphous phase becomes a carrier of the deformation. In fact, the studies that are now accumulating on a varied range of materials reveal more complex situations where amorphization intervenes as one deformation mechanism among others, and often in interaction with the others. The link with grain boundary sliding is a good illustration. In some cases the grain boundary sliding triggers the formation of shear bands ([82], see Fig. 18), elsewhere the amorphization is the grain boundary sliding mechanism that will require other mechanisms of intragranular accommodations to avoid damage ([41], see Fig. 15) or conversely, the presence of amorphous films at the grain boundary will accommodate the absorption of dislocations from the grains ([102], see Fig. 16). These observations lead us to suggest that stress-induced amorphization should be considered a deformation

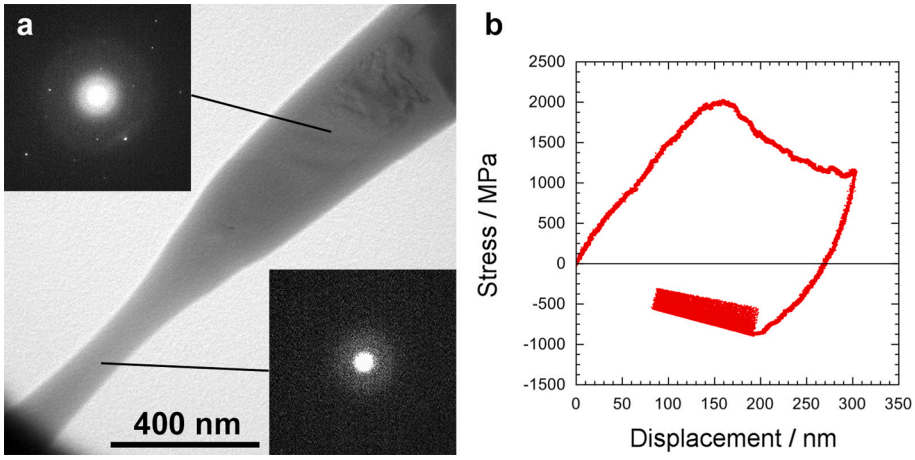


**Fig. 22.** Amorphization during elongation of a quartz micropillar (Modified after [130] with permission of the authors). a) TEM image after elongation resulting from adherence of the micropillar with the retracted flat punch (bottom left corner). b) engineering stress versus displacement showing the compression and elongation stages.

mechanism in its own right.

It is striking that very few studies have been devoted to the rheology of the amorphous materials created by this process. Some have focused on the density of the produced amorphous material [75]. Demkowicz and Argon [35] distinguished two types of amorphous Si: "solid-like" and "fluid-like" without further specifying their properties. Only a few studies lead to information about the viscosities although they play a fundamental role on the capacity of the amorphous material to produce deformation.

Temperature affects the viscosity of glasses considerably. However, no study has been made to investigate the influence of this parameter, neither on the amorphization, nor on the resulting deformation. In fact, most of the experiments reported in this review were done at low temperature (in practice room temperature for rather refractory materials). Exceptions are the shock experiments which are always accompanied by a temperature rise, but this is rarely considered. We note however, with minerals, the experiments of Girard *et al.* [44] on bridgmanite, and Bollinger *et al.* [12] and Gasc *et al.* [41] on olivine, which were carried out at temperatures higher than ambient. For olivine, the temperatures investigated are in the range 0.6–0.7 $T_m$ ($T_m$ being the melting temperature) for Gasc *et al.* and 0.5–0.6 $T_m$ for Bollinger *et al.* (due to the pressure effect on $T_m$) which corresponds to low temperature plasticity for this silicate. For bridgmanite, the experiments correspond to about 0.75 $T_m$. For olivine, the interesting point to note is the influence of the glass transition temperature on the mechanical behavior of the material subjected to amorphization. Samae *et al.* [109] suggest that the rheological transition associated with this effect could account in the Earth for the viscosity drop between the lithosphere and asthenosphere. Thus, stress-induced amorphization could be an important mechanism in geodynamics. This hypothesis remains to be confirmed, in particular by observations of natural materials. In this context, we note with interest the observation of a nanosized intra-granular amorphous phase in the eclogite omphacite of the Dabieshan UHP metamorphic belt reported by Su *et al.* [123]. This invites a search for other natural occurrences of this mechanism that could be important in geodynamics in high-stress settings.

## CRediT authorship contribution statement

**Hosni Idrissi:** Funding acquisition, conceptualization, original draft writing, review & editing. **Philippe Carrez:** Original draft writing, review & editing. **Patrick Cordier:** Funding acquisition, conceptualization, original draft writing, review & editing.

## Declaration of Competing Interest

The authors declare that they have no known competing financial interests or personal relationships that could have appeared to influence the work reported in this paper.

## Acknowledgements

H. Idrissi is mandated by the Belgian National Fund for Scientific Research (FSR- FNRS). This work was supported by the FNRS under Grant CDR – J.0113.20 and by the European Research Council (ERC) under the European Union's Horizon 2020 research and innovation programme under grant agreement No 787,198 – TimeMan.

## References

[1] Y. Akahama, Y. Mori, M. Kobayashi, H. Kawamura, K. Kimura, S. Takeuchi, Pressure-Induced Amorphization of Quasi Crystals, J. Phys. Soc. Japan 58 (7) (1989) 2231–2234, https://doi.org/10.1143/JPSJ.58.2231.

[2] L.W. Alvarez, W. Alvarez, F. Asaro, H.V. Michel, Extraterrestrial cause for the Cretaceous- Tertiary extinction, Science 208 (4448) (1980) 1095–1108, https://doi.org/10.1126/science.208.4448.1095.

[3] Q. An, K.M. Reddy, J. Qian, K.J. Hemker, M.W. Chen, W.A. Goddard III, Nucleation of amorphous shear bands at nanotwins in boron suboxide, Nature Comm. 7 (2016) 11001, https://doi.org/10.1038/ncomms11001.

[4] D. Andrault, M.A. Bouhifd, J.P. Itie, P. Richet, Compression and amorphization of $(Mg, Fe)_2SiO_4$ olivines: An X-ray diffraction study up to 70 GPa, Phys. Chem. Minerals 22 (1995) 99–107, https://doi.org/10.1007/BF00202469.

[5] C.A. Angell, Formation of glasses from liquids and biopolymers, Science 267 (5206) (1995) 1924–1935, https://doi.org/10.1126/science.267.5206.1924.

[6] J. Badro, J.L. Barrat, P.h. Gillet, Numerical simulation of α-quartz under non-hydrostatic compression. Memory glass and five-coordinated crystalline phases, Phys. Rev. Lett. 76 (1995) 772–775, https://doi.org/10.1103/PhysRevLett.76.772.

[7] T.H.K. Barron, M.L. Klein, Second-order elastic constants of a solid under stress, Proc. Phys. Soc. 85 (3) (1965) 523–532, https://doi.org/10.1088/0370-1328/85/3/313.

[8] N. Binggeli, N.R. Keskar, J.R. Chelikowsky, Pressure-induced amorphization, elastic instability, and soft modes in alpha-quartz, Phys. Rev. B 49 (1994) 3075–3081, https://doi.org/10.1103/PhysRevB.49.3075.

[9] M.J. Bloch, Effet de l'irradiation par les neutrons sur les alliages uranium-fer a faible teneur en fer, J. Nucl. Mater. 6 (2) (1962) 203–212, https://doi.org/10.1016/0022-3115(62)90271-4.

[10] S.V. Bobylev, I.A. Ovid'ko, Nanoscale amorphization at disclination quadrupoles in deformed nanomaterials and polycrystals, Appl. Phys. Lett. 93 (6) (2008) 061904, https://doi.org/10.1063/1.2953448.

[11] B.F. Bohor, P.J. Modreski, E.E. Foord, Shocked quartz in the Cretaceous/Tertiary boundary clays: evidence for a global distribution, Science 236 (1987) 705–708, https://doi.org/10.1126/science.236.4802.705.

[12] C. Bollinger, K. Marquardt, F. Ferreira, Intragranular plasticity vs. grain boundary sliding (GBS) in forsterite: microstructural evidence at high pressures (3.5-5.0 GPa), Am. Mineral. 104 (2) (2019) 220–231, https://doi.org/10.2138/am-2019-6629.

[13] I.Y. Borg (1972) Some shock effects in granodiorite to 270 kilobars at the Piledriver site. In Flow and Fracture of Rocks. (1972), Geophys. Monogr. Ser., vol. 16, edited by H. C. Heard *et al.*, pp. 293-311, AGU, Washington, D. C. Doi: 10.1029/GM016p0293.

[14] M. Born, Thermodynamics of Crystals and Melting, J. Chem. Phys. 7 (8) (1939) 591–603, https://doi.org/10.1063/1.1750497.

[15] M. Born, On the stability of crystal lattices. I, Mathematical Proceedings of the Cambridge Philosophical Society 36 (2) (1940) 160–172, https://doi.org/10.1017/S0305004100017138.

[16] P.S. Branício, J.-P. Rino, Large deformation and amorphization of Ni nanowires under uniaxial strain A molecular dynamics study, J. Phys. Rev. B 62 (24) (2000) 16950–16955, https://doi.org/10.1103/PhysRevB.62.16950.

[17] W.C. Broegger, Salmonsens Store Illustrerede Konversationsleksikon 1 (1893) 742.

[18] A. Calka, A.P. Radlinski, Formation of amorphous Fe-B alloys by mechanical alloying, Appl. Phys. Lett. 58 (2) (1991) 119–121, https://doi.org/10.1063/1.104974.

[19] E.C.T. Chao, Shock effects of certain rock forming minerals, Science 156 (1967) 192–202, https://doi.org/10.1126/science.156.3772.192.

[20] E.C.T. Chao, O.B. James, J.A. Minkin, J.A. Boreman, E.D. Jackson, C.B. Raleigh, Petrology of unshocked crystalline rocks and evidence of impact metamorphism in Apollo 11 returned lunar sample, Geochim. Cosrnochim. Acta Suppl. 1 (1970) 287–314.

[21] S.Z. Chavoshi, P.S. Branicio, Q. An, Transition between Hall-Petch and inverse Hall-Petch behavior in nanocrystalline silicon carbide, Phys. Rev. Materials 5 (2021), 073606, https://doi.org/10.1103/PhysRevMaterials.5.073606.

[22] J.R. Chelikowsky, N. Troullier, J.L. Martins, H.E. King Jr., Pressure dependence of the structural properties of α-quartz near the amorphous transition, Phys. Rev. B 44 (1991) 489–497, https://doi.org/10.1103/PhysRevB.44.489.

[23] M.W. Chen, McCauley, K.J. Hemker, Shock-Induced Localized Amorphization in Boron Carbide, Science 299 (2003) 1563–1566, https://doi.org/10.1126/science.1080819.

[24] H. Chen, V.I. Levitas, L. Xiong, Amorphization induced by 60° shuffle dislocation pileup against different grain boundaries in silicon bicrystal under shear, Acta Mater. 179 (2019) 287–295, https://doi.org/10.1016/j.actamat.2019.08.023.

[25] N. Choudhury, S.L. Chaplot, Ab initio studies of phonon softening and high-pressure phase transitions of α-quartz $SiO_2$, Phys. Rev. B 73 (2006), 094304, https://doi.org/10.1103/PhysRevB.73.094304.

[26] D.R. Clarke, M.C. Kroll, P.D. Kirchner, R.F. Cook, B.J. Hockey, Amorphization and Conductivity of Silicon and Germanium Induced by Indentation, Phys. Rev. Lett. 60 (21) (1988) 2156–2159, https://doi.org/10.1103/PhysRevLett.60.2156.

[27] D.M. Clatterbuck, C.R. Krenn, M.L. Cohen, J.W. Morris Jr., Phonon Instabilities and the Ideal Strength of Aluminum, Phys. Rev. Lett. 91 (2003), 135501, https://doi.org/10.1103/PhysRevLett.91.135501.

[28] P. Cordier, J.C. Doukhan, J. Peyronneau, Structural transformations of quartz and berlinite $AlPO_4$ at high pressure and room temperature: a transmission electron microscopy study, Phys. Chem. Minerals 20 (1993) 176–189, https://doi.org/10.1007/BF00200120.

[29] P. Cordier, A.J. Gratz, TEM study of shock metamorphism in quartz from the Sedan nuclear test site, Earth Planet. Sci. Lett. 129 (1–4) (1995) 163–170, https://doi.org/10.1016/0012-821X(94)00243-R.

[30] P. Cordier, D.C. Rubie, Plastic deformation under extreme pressure using a multi-anvil apparatus, Mat. Sci. Eng. A 309-310 (2001) 38–43, https://doi.org/10.1016/S0921-5093(00)01795-0.

[31] F. Dachille, R.J. Zeto, R. Roy, Coesite and Stishovite: Stepwise Reversal Transformations, Science 140 (3570) (1963) 991–993, https://doi.org/10.1126/science.140.3570.991.

[32] D.W. Dean, R.M. Wentzcovitch, N. Keskar, J.R. Chelikowsky, N. Binggeli, Pressure-induced amorphization in crystalline silica: Soft phonon modes and shear instabilities in coesite, Phys. Rev. B 61 (5) (2000) 3303–3309, https://doi.org/10.1103/PhysRevB.61.3303.

[33] P.S. De Carli, D.J. Milton, Stishovite: synthesis by shock wave, Science 147 (3654) (1965) 144–145, https://doi.org/10.1126/science.147.3654.144.

[34] M.J. Demkowicz, A.S. Argon, High-Density Liquidlike Component Facilitates Plastic Flow in a Model Amorphous Silicon System, Phys. Rev. Lett. 93 (2004), 025505, https://doi.org/10.1103/PhysRevLett.93.025505.

[35] M.J. Demkowicz, A.S. Argon, Liquidlike atomic environments act as plasticity carriers in amorphous silicon, Phys. Rev. B 72 (2005), 245205, https://doi.org/10.1103/PhysRevB.72.245205.

[36] M.J. Demkowicz, A.S. Argon, D. Farkas, M. Frary, Simulation of plasticity in nanocrystalline silicon, Philos. Mag. 87 (28) (2007) 4253–4271, https://doi.org/10.1080/14786430701358715.

[37] D.J. Durben, P.F. McMillan, G.H. Wolf, Raman study of the high-pressure behavior of forsterite ($Mg_2SiO_4$) crystal and glass, Am. Mineral. 78 (1993) 1143–1148.

[38] W.V. Engelhardt, J. Arndt, D. Stöffler, W.F. Müller, H. Jeziorkowski, R.A. Gubser, Diaplektische Gläser in den Breccien des Ries von Nördlingen als Anzeichen von Stoßwellenmetamorphose, Contrib. Mineral. Petrol. 15 (1967) 93–102, https://doi.org/10.1007/BF01167216.

[39] W. von Engelhardt, W. Bertsch, Shock induced planardeformation structures in quartz from the Ries crater, Germany. Contrib. Mineral. Petrol. 20 (1969) 203–234, https://doi.org/10.1007/BF00377477.

[40] J. Frenkel, Zur Theorie der Elastizitätsgrenze und der Festigkeit kristallinischer Körper, Z. Physik 37 (1926) 572–609, https://doi.org/10.1007/BF01397292.

[41] J. Gasc, S. Demouchy, F. Barou, S. Koizumi, P. Cordier, Creep mechanisms in the lithospheric mantle Inferred from deformation of iron-free forsterite aggregates at 900–1200 °C, Tectonophysics 761 (2019) 16–30, https://doi.org/10.1016/j.tecto.2019.04.009.

[42] J.J. Gilvarry, The Lindemann and Grüneisen laws, Phys. Rev. 102 (1956) 308–316, https://doi.org/10.1103/PhysRev.102.308.

[43] D. Ghosh, G. Subhash, T.S. Sudarshan, R. Radhakrishnan, X.-L. Gao, Dynamic indentation response of fine-grained boron carbide, J. Am. Ceram. Soc. 90 (6) (2007) 1850–1857, https://doi.org/10.1111/j.1551-2916.2007.01652.x.

[44] J. Girard, G. Amulele, R. Farla, A. Mohiuddin, S.-I. Karato, Shear deformation of bridgmanite and magnesiowüstite aggregates at lower mantle conditions, Science 351 (6269) (2016) 144–147, https://doi.org/10.1126/science.aad3113.

[45] K. Gouriet, P. Carrez, P. Cordier, Ultimate Mechanical Properties of Forsterite, Ultimate Mechanical Properties of Forsterite. Minerals. 9 (12) (2019) 787, https://doi.org/10.3390/min9120787.

[46] D.E. Grady, Shock deformation of brittle solids, J. Geophys. Res. 85 (1980) 913–924, https://doi.org/10.1029/JB085iB02p00913.

[47] A.J. Gratz, Deformation in laboratory-shocked quartz, J. Non Cryst. Solids 67 (1984) 543–558, https://doi.org/10.1016/0022-3093(84)90175-3.

[48] A.J. Gratz, J. Tyburczy, J. Christie, T. Ahrens, P. Pongratz, Shock metamorphism of deformed quartz, Phys Chem. Minerals 16 (1988) 221–233, https://doi.org/10.1007/BF00220689.

[49] A.J. Gratz, W.J. Nellis, J.M. Christie, W. Brocious, J. Swegle, P. Cordier, Shock metamorphism of quartz with initial temperatures -170 to +1000°C, Phys. Chem. Minerals 19 (1992) 267–288, https://doi.org/10.1007/BF00204005.

[50] S.-H. Guan, X.-J. Zhang, Z.-P. Liu, Energy Landscape and Crystal-to-Crystal Transition of Ternary Silicate $Mg_2SiO_4$, J. Phys. Chem. C 120 (43) (2016) 25110–25116, https://doi.org/10.1021/acs.jpcc.6b08942.

[51] M.Y. Gutkin, I.A. Ovid'ko, Plastic Flow in amorphous covalent solids and nanoceramics with amorphous intergranular layers, Rev. Adv. Mater. Sci. 21 (2009) 139–154.

[52] D. Guo, S. Song, R. Luo, W.A. Goddard III, M. Chen, K.M. Reddy, Q. An, Grain Boundary Sliding and Amorphization are Responsible for the Reverse Hall-Petch Relation in Superhard Nanocrystalline Boron Carbide, Phys. Rev. Lett. 121 (2018), 145504, https://doi.org/10.1103/PhysRevLett.121.145504.

[53] F. Guyot, B. Reynard, Pressure-induced structural modifications and amorphization in olivine compounds, Chemical Geology 96 (3-4) (1992) 411–420, https://doi.org/10.1016/0009-2541(92)90069-H.

[54] J. Han, S. Xu, J. Sun, L. Fang, H. Zhu, Pressure-induced amorphization in the nanoindentation of single crystalline silicon, Pressure-induced amorphization in the nanoindentation of single crystalline silicon RSC Adv. 7 (3) (2017) 1357–1362, https://doi.org/10.1039/C6RA26094B.

[55] X.D. Han, Y.F. Zhang, K. Zheng, X.N. Zhang, Z. Zhang, Y.J. Hao, X.Y. Guo, J. Yuan, Z.L. Wang, Low-Temperature in Situ Large Strain Plasticity of Ceramic SiC Nanowires and Its Atomic-Scale Mechanism, Nano Lett. 7 (2) (2007) 452–457, https://doi.org/10.1021/nl0627689.

[56] A. Hamberg, Die radioaktiven Substanzen und die geologische Forschung, Geologiska Foereningan i Stockholm. Foerhandlingar 36 (1914) 31–96.

[57] R.M. Hazen, L.W. Finger, R.J. Hemley, H.K. Mao, High-pressure crystal chemistry and amorphization of α-quartz, Solid State Communications. 72 (5) (1989) 507–511, https://doi.org/10.1016/0038-1098(89)90607-8.

[58] Y. He, L.i. Zhong, F. Fan, C. Wang, T. Zhu, S.X. Mao, In situ observation of shear-driven amorphization in silicon crystals, Nature Nanotechnology. 11 (10) (2016) 866–871, https://doi.org/10.1038/nnano.2016.166.

[59] R.J. Hemley, A.P. Jephcoat, H.K. Mao, L.C. Ming, M.H. Manghnani, Pressure-induced amorphization of crystalline silica, Nature 334 (6177) (1988) 52–54, https://doi.org/10.1038/334052a0.

[60] R. Hill, On the elasticity and stability of perfect crystals at finite strain, Mathematical Proceedings of the Cambridge Philosophical Society 77 (1) (1975) 225–240, https://doi.org/10.1017/S0305004100049549.

[61] K. Hirose, N. Takafuji, K. Fujino, S.R. Shieh, T.S. Duffy, Iron partitioning between perovskite and post-perovskite: A transmission electron microscope study, Am. Mineral. 93 (10) (2008) 1678–1681, https://doi.org/10.2138/am.2008.3001.

[62] J.Y. Huang, H. Yasuda, H. Mori, Deformation-induced amorphization in ball-milled silicon, Philos. Mag. Lett. 79 (6) (1999) 305–314, https://doi.org/10.1080/095008399177147.

[63] J.Y. Huang, Y.T. Zhu, X.Z. Liao, R.Z. Valiev, Amorphization of TiNi induced by high-pressure torsion, Philos. Mag. Lett. 84 (3) (2004) 183–190, https://doi.org/10.1080/09500830310001657353.

[64] A.R. Huffman, J.M. Brown, N.L. Carter, W.U. Reimold, The microstructural response of quartz and feldspar under shock loading at variable temperatures, J. Geophys. Res. 98 (B12) (1993) 22171–22197, https://doi.org/10.1029/93JB01425.

[65] H. Ikeda, Y. Qi, T. Çagin, K. Samwer, W.L. Johnson, W.A. Goddard, Strain Rate Induced Amorphization in Metallic Nanowires, Phys. Rev. Lett. 82 (14) (1999) 2900–2903, https://doi.org/10.1103/PhysRevLett.82.2900.

[66] M. Ishimaru, I.-T. Bae, Y. Hirotsu, Electron-beam-induced amorphization in SiC, Phys. Rev. B 68 (2003), 144102, https://doi.org/10.1103/PhysRevB.68.144102.

[67] R. Jeanloz, T.J. Ahrens, J.S. Lally, G.L. Nord, J.M. Christie, A.H. Heuer, Shock-Produced Olivine Glass: First Observation, Science 197 (4302) (1977) 457–459, https://doi.org/10.1126/science.197.4302.457.

[68] K.J. Kingma, C. Meade, R.J. Hemley, H.-K. Mao, D.R. Veblen, Microstructural Observations of α-Quartz Amorphization, Science 259 (5095) (1993) 666–669, https://doi.org/10.1126/science.259.5095.666.

[69] C.C. Koch, J.D. Whittenberger, Mechanical milling/alloying of intermetallics, Intermetallics. 4 (5) (1996) 339–355, https://doi.org/10.1016/0966-9795(96)00001-5.

[70] M. Kohyama, Tensile strength and fracture of a tilt grain boundary in cubic SiC: A first-principles study, Philos. Mag. Lett. 79 (9) (1999) 659–672, https://doi.org/10.1080/095008399176706.

[71] M. Kohyama, Ab initio study of the ttensile strength and fracture of coincidence tilt boundaries in cubic SiC: polar interfaces of the {122} Σ=9 boundary, Phys. Rev. B 65 (2002), 184107, https://doi.org/10.1103/PhysRevB.65.184107.

[72] K. Kranjc, A.S. Thind, A.Y. Borisevich, R. Mishra, R.M.P. Skemer Flores, Amorphization and plasticity of olivine during low-temperature micropillar deformation experiments, J. Geophys. Res. Solid Earth 125 (2020), e2019JB019242, https://doi.org/10.1029/2019JB019242.

[73] F. Langenhorst, Shock experiments on pre-heated α- and β-quartz: II. X-ray and TEM investigations, Earth Planet. Sci. Lett. 128 (3-4) (1994) 683–698, https://doi.org/10.1016/0012-821X(94)90179-1.

[74] F. Langenhorst, A. Deutsch, Shock experiments on pre-heated α- and β-quartz: I. Optical and density data Earth Planet, Sci. Lett. 125 (1-4) (1994) 407–420, https://doi.org/10.1016/0012-821X(94)90229-1.

[75] V.I. Levitas, Y. Ma, E. Selvi, J. Wu, J.A. Patten, High-density amorphous phase of silicon carbide obtained under large plastic shear and high pressure, Phys. Rev. B 85 (5) (2012), 054114, https://doi.org/10.1103/PhysRevB.85.054114.

[76] Z.C. Li, L. Liu, X. Wu, L.L. He, Y.B. Xu, Indentation induced amorphization in gallium arsenide, Mater. Sci. Eng. A 337 (1–2) (2002) 21–24, https://doi.org/10.1016/S0921-5093(02)00015-1.

[77] D.J. Li, J.T. Wang, B.Z. Ding, The amorphization of the Cd-Sb system by high pressure, Scripta Metal. Mater. 26 (4) (1992) 621–626, https://doi.org/10.1016/0956-716X(92)90295-P.

[78] J. Li, S. Yip, Atomistic Measures of Materials Strength, Comp. Model. Eng. Sci. 3 (2002) 219–227, https://www.techscience.com/CMES/v3n2/24766.

[79] Z.J. Lin, M.J. Zhuo, Z.Q. Sun, P. Veyssière, Y.C. Zhou, Amorphization by dislocation accumulation in shear bands, Acta Mater. 57 (9) (2009) 2851–2857, https://doi.org/10.1016/j.actamat.2009.02.040.

[80] F.A. Lindemann, Über die Berechnung molekularer Eigenfrequenzen, Phys. Zeitsch 11 (1910) 609–612.

[81] G.-H. Lu, S. Deng, T. Wang, M. Kohyama, R. Yamamoto, Theoretical tensile strength of an Al grain boundary, Phys. Rev. B 69 (2004), 134106, https://doi.org/10.1103/PhysRevB.69.134106.

[82] H. Luo, H. Sheng, H. Zhang, F. Wang, J. Fan, J. Du, J.P. Liu, I. Szlufarska, Plasticity without dislocations in a polycrystalline intermetallic, Nature Comm. 10 (2019) 3587, https://doi.org/10.1038/s41467-019-11505-1.

[83] H. Luo, H. Zhang, H. Sheng, J.P. Liu, I. Szlufarska, Amorphous shear bands in $SmCo_5$, Mater. Sci. Eng. A. 785 (2020) 139340, https://doi.org/10.1016/j.msea.2020.139340.

[84] C. Meade, R. Jeanloz, Yield strength of MgO to 40 GPa, J. Geophys. Res. 93 (1988) 3261–3269, https://doi.org/10.1029/JB093iB04p03261.

[85] C. Meade, R. Jeanloz, R.J. Hemley, Spectroscopic and X-Ray Diffraction Studies of Metastable Crystalline-Amorphous Transitions in $Ca(OH)_2$ and Serpentine. In High-Pressure Research: Application to Earth and Planetary Sciences (eds Y. Syono and M.H. Manghnani). (1992), https://doi.org/10.1029/GM067p0485.

[86] D. Machon, F. Meersman, M.C. Wilding, M. Wilson, P.F. McMillan, Pressure-induced amorphization and polyamorphism: Inorganic and biochemical systems, Progress Mater. Sci. 61 (2014) 216–282, https://doi.org/10.1016/j.pmatsci.2013.12.002.

[87] D. Machon, P. Mélinon, Size-dependent pressure-induced amorphization: a thermodynamic panorama, Phys. Chem. Chem. Phys. 17 (2) (2015) 903–910, https://doi.org/10.1039/C4CP04633A.

[88] D.J. Milton, P.S. De Carli, Maskelynite: formation by explosive shock, Science 140 (3567) (1963) 670–671, https://doi.org/10.1126/science.140.3567.670.

[89] K. Minowa, K. Sumino, Stress-Induced Amorphization of a Silicon Crystal by Mechanical Scratching, Phys. Rev. Lett. 69 (1992) 320, https://doi.org/10.1103/physrevlett.69.320.

[90] O. Mishima, L.D. Calvert, E. Whalley, 'Melting' ice I at 77 K and 10 kbar: a new method of making amorphous solids, Nature 310 (1984) 393–395, https://doi.org/10.1038/310393a0.

[91] O. Mishima, Relationship between melting and amorphization of ice, Nature 384 (6609) (1996) 546–549, https://doi.org/10.1038/384546a0.

[92] L. Miyagi, W. Kanitpanyacharoen, P. Kaercher, S. Stackhouse, B. Militzer, H.-R. Wenk, The enigma of post-perovskite anisotropy: deformation versus transformation textures, Phys. Chem. Minerals 38 (2011) 665–678, https://doi.org/10.1007/s00269-011-0439-y.

[93] K. Mizushima, S. Yip, E. Kaxiras, Ideal crystal stability and pressure-induced phase transition in silicon, Phys. Rev. B 50 (20) (1994) 14952–14959, https://doi.org/10.1103/PhysRevB.50.14952.

[94] F. Mouhat, F.X. Coudert, Necessary and sufficient elastic stability conditions in various crystal systems, Phys. Rev. B 90 (22) (2014), 224104, https://doi.org/10.1103/PhysRevB.90.224104.

[95] W.F. Müller, W. Défourneaux, Deformationsstrukturen in Quarz als Indikator für Stosswellen: eine experiimentelle Untersuchung an Quarzeinkristallen, Z. Geophys. 34 (1968) 483–504.

[96] K. Nakamura, T. Mizoguchi, N. Shibata, K. Matsunaga, T. Yamamoto, Y. Ikuhara, First-principles study of grain boundary sliding in $\alpha-Al_2O_3$, Phys. Rev. B 75 (2007), 184109, https://doi.org/10.1103/PhysRevB.75.184109.

[97] S.-W. Nam, H.-S. Chung, Y.C. Lo, L. Qi, J.u. Li, Y.e. Lu, A.T.C. Johnson, Y. Jung, P. Nukala, R. Agarwal, Electrical Wind Force-Driven and Dislocation-Templated Amorphization in Phase-Change Nanowires, Science 336 (6088) (2012) 1561–1566, https://doi.org/10.1126/science.1220119.

[98] B.C. Nzogang, J. Bouquerel, P. Cordier, A. Mussi, J. Girard, S. Karato, Characterization by scanning precession electron diffraction of an aggregate of bridgmanite and ferropericlase deformed at HP-HT, Geochem. Geophys. Geosyst. 19 (3) (2018) 582–594, https://doi.org/10.1002/2017GC007244.

[99] S. Ogata, N. Hirosaki, C. Kocer, H. Kitagawa, An ab initio calculation of the ideal tensile strength of β-silicon nitride, Phys. Rev. B 64 (2001), 172102, https://doi.org/10.1103/PhysRevB.64.172102.

[100] S. Ogata, Y. Umeno, M. Kohyama, First-principles approaches to intrinsic strength and deformation of materials: perfect crystals, nano-structures, surfaces and interfaces, Modelling Simul. Mater. Sci. Eng. 17 (1) (2009) 013001, https://doi.org/10.1088/0965-0393/17/1/013001.

[101] I.A. Ovid'ko, Nanoscale amorphization as a special deformation mode in nanowires, Scripta Mater 66 (2012) 402–405. http://dx.doi.org/10.1016/j.scriptamat.2011.12.001.

[102] Z. Pan, T.J. Rupert, Amorphous intergranular films as toughening structural features, Acta Mater. 89 (2015) 205–214, https://doi.org/10.1016/j.actamat.2015.02.012.

[103] M. Peterlechner, T. Waitz, H.P. Karnthaler, Nanoscale amorphization of severely deformed NiTi shape memory alloys, Scripta Mater. 60 (12) (2009) 1137–1140, https://doi.org/10.1016/j.scriptamat.2009.02.055.

[104] J.P. Poirier, Dislocation-mediated melting of iron and the temperature of the Earth's core, Geophys. J. R. Astron. Soc. 58 (1986) 315–328, https://doi.org/10.1111/j.1365-246X.1986.tb04515.x.

[105] J.P. Poirier, G.D. Price, Dislocation melting of metals, Phys. Earth Planet. Int. 69 (3–4) (1992) 153–162, https://doi.org/10.1016/0031-9201(92)90131-E.

[106] K.M. Reddy, D. Guo, S. Song, C. Cheng, J. Han, X. Wang, Q. An, M. Chen, Dislocation-mediated shear amorphization in boron carbide, Sci. Adv. 7 (8) (2021), eabc6714, https://doi.org/10.1126/sciadv.abc6714.

[107] K.M. Reddy, P. Liu, A. Hirata, T. Fujita, M.W. Chen, Atomic structure of amorphous shear bands in boron carbide, Nature Comm. 4 (2013) 2483, https://doi.org/10.1038/ncomms3483.

[108] G. Richard, P. Richet, Room-temperature amorphization of fayalite and high-pressure properties of $Fe_2SiO_4$ liquid, Geophys. Res. Lett. 17 (12) (1990) 2093–2096, https://doi.org/10.1029/GL017i012p02093.

[109] V. Samae, P. Cordier, S. Demouchy, C. Bollinger, J. Gasc, S. Koizumi, A. Mussi, D. Schryvers, H. Idrissi, Stress-induced amorphization triggers deformation in the lithospheric mantle, Nature 591 (7848) (2021) 82–86, https://doi.org/10.1038/s41586-021-03238-3.

[110] D. Santamaria-Perez, A. Thomson, A. Segura, J. Pellicer-Torres, F.J. Manjon, F. Corà, K. McColl, M. Wilson, D. Dobson, P.F. McMillan, Metastable structural transformations and pressure-induced amorphization in natural $(Mg, Fe)_2SiO_4$ olivine under static compression: A Raman spectroscopic study, Am. Mineral. 101 (7) (2016) 1642–1650, https://doi.org/10.2138/am-2016-5389CCBY.

[111] X. Sauvage, L. Renaud, B. Deconihout, D. Blavette, D.H. Ping, K. Hono, Solid state amorphization in cold drawn Cu/Nb wires, Acta Mater. 49 (3) (2001) 389–394, https://doi.org/10.1016/S1359-6454(00)00338-4.

[112] J.D. Schuler, O.K. Donaldson, T.J. Rupert, Amorphous complexions enable a new region of high temperature stability in nanocrystalline Ni-W, Scripta Mater. 154 (2018) 49–53, https://doi.org/10.1016/j.scriptamat.2018.05.023.

[113] Z. Shan, E.A. Stach, J.M.K. Wiezorek, J.A. Knapp, D.M. Follstaedt, S.X. Mao, Grain boundary-mediated plasticity in nanocrystalline nickel, Science 305 (5684) (2004) 654–657, https://doi.org/10.1126/science.1098741.

[114] N.M. Short, Effects of shock pressures from a nuclear explosion on mechanical and optical properties of granodiorite, J. Geophys. Res. 71 (4) (1966) 1195–1215, https://doi.org/10.1029/JZ071i004p01195.

[115] N.M. Short, Progressive shock metamorphism of quartzite ejecta from the Sedan nuclear explosion crater, J. Geol. 78 (6) (1970) 705–732, https://doi.org/10.1086/627572.

[116] B.J. Skinner, J.J. Fahey, Observations on the Inversion of Stishovite to Silica Glass, J. Geophys. Res. 68 (19) (1963) 5595–5604, https://doi.org/10.1029/JZ068i019p05595.

[117] M. Šob, L.G. Wang, V. Vitek, Theoretical tensile stress in tungsten single crystals by full-potential first-principles calculations, Mater. Sci. Eng. A 234–236 (1997) 1075–1078, https://doi.org/10.1016/S0921-5093(97)00329-8.

[118] D. Stöffler, Anzeichen besonderer mechanischer Beanspruchung an Mineralien des Kristallineinschlusse des Suevits (Stosswellenmetamorphose), N. Jb. Miner Mh. 9–11 (1965) 350–354.

[119] D. Stöffler, Progressive metamorphism and classification of shocked and brecciated crystalline rocks at impact craters, J. Geophys. Res. 76 (23) (1971) 5541–5551, https://doi.org/10.1029/JB076i023p05541.

[120] D. Stöffler, U. Hornemann, Quartz and feldspar glasses produced by natural and experimental shock, Meteoritics 7 (3) (1972) 371–394, https://doi.org/10.1111/j.1945-5100.1972.tb00449.x.

[121] D. Stöffler, C. Hamann, K. Metzler, Shock metamorphism of planetary silicate rocks and sediments: Proposal for an updated classification system, Meteoritics Planet. Sci. 53 (1) (2018) 5–49, https://doi.org/10.1111/maps.12912.

[122] E.M. Stolper, T.J. Ahrens, On the nature of pressure-induced coordination changes in silicate melts and glasses, Geophys. Res. Lett. 14 (12) (1987) 1231–1233, https://doi.org/10.1029/GL014i012p01231.

[123] W. Su, M. Zhang, J. Chen, G.D. Bromiley, K. Ye, S.A.T. Redfern, J. Lin, Amorphization in natural omphacite and its implications, J. Asian Earth Sci. 42 (4) (2011) 694–703, https://doi.org/10.1016/j.jseaes.2010.10.001.

[124] G. Subhash, A.P. Awasthi, C. Kunka, P. Jannotti, M. DeVries, In search of amorphization-resistant boron carbide, Scripta Mater. 123 (2016) 158–162, https://doi.org/10.1016/j.scriptamat.2016.06.012.

[125] C. Suryanarayana, Mechanical alloying and milling, Progress Mater. Sci. 46 (1–2) (2001) 1–184, https://doi.org/10.1016/S0079-6425(99)00010-9.

[126] T. Suzuki, T. Ohmura, Ultra-microindentation of silicon at elevated temperatures, Philos. Mag. A 74 (5) (1996) 1073–1084, https://doi.org/10.1080/01418619608239708.
[127] I. Szlufarska, R.K. Kalia, A. Nakano, P. Vashishta, Nanoindentation-induced amorphization in silicon carbide, Appl. Phys. Lett. 85 (3) (2004) 378–380, https://doi.org/10.1063/1.1774252.
[128] I. Szlufarska, A. Nakano, P. Vashishta, A Crossover in the Mechanical Response of Nanocrystalline Ceramics, Science 309 (5736) (2005) 911–914, https://doi.org/10.1126/science.1114411.
[129] H. Tait, Five thousand years of glass, British Museum press, London, 1991.
[130] E. Tochigi, E. Zepeda-alarcon, H.-R. Wenk, A.M. Minor, In situ TEM observations of plastic deformation in quartz crystals, Phys. Chem. Minerals 41 (10) (2014) 757–765, https://doi.org/10.1007/s00269-014-0689-6.
[131] S.J. Tracy, S.J. Turneaure, T.S. Duffy, Structural response of -quartz under plate-impact shock compression, Sci. Adv. 6 (2020) eabb3913, https://doi.org/10.1126/sciadv.abb3913.
[132] M. Tang, S. Yip, Atomic Size Effects in Pressure-Induced Amorphization of a Binary Covalent Lattice, Phys. Rev. Lett. 75 (14) (1995) 2738–2741, https://doi.org/10.1103/PhysRevLett.75.2738.
[133] T.J. Vogler, W.D. Reinhart, L.C. Chhabildas, Dynamic behavior of boron carbide, J. Appl. Phys. 95 (2004) 4173, https://doi.org/10.1063/1.1686902.
[134] D. Wales, Energy Landscapes: Applications to Clusters, Biomolecules and Glasses (Cambridge Molecular Science), Cambridge University Press, Cambridge, 2003, https://doi.org/10.1017/CBO9780511721724.
[135] Y. Wang, W.B. Durham, I.C. Getting, D.J. Weidner, The deformation-DIA: A new apparatus for high temperature triaxial deformation to pressures up to 15 GPa, Rev. Sci. Inst. 74 (6) (2003) 3002–3011, https://doi.org/10.1063/1.1570948.
[136] J. Wang, J.u. Li, S. Yip, S. Phillpot, D. Wolf, Mechanical instabilities of homogeneous crystals, Phys. Rev. B 52 (17) (1995) 12627–12635, https://doi.org/10.1103/PhysRevB.52.12627.
[137] H.-R. Wenk, S. Matthies, R.J. Hemley, H.-K. Mao, J. Shu, The plastic deformation of iron at pressures of the Earth's inner core, Nature 405 (6790) (2000) 1044–1047, https://doi.org/10.1038/35016558.
[138] R.M. Wentzcovitch, C. da Silva, J.R. Chelikowsky, N.A. Binggeli, New phase and pressure induced amorphization in silica, Phys. Rev. Lett. 80 (1998) 2149–2152, https://doi.org/10.1103/PhysRevLett.80.2149.
[139] Q. Williams, R. Jeanloz, Static amorphization of anorthite at 300 K and comparison with diaplectic glass, Nature 338 (6214) (1989) 413–415, https://doi.org/10.1038/338413a0.
[140] Y. Wu, Y. Xu, Lattice-distortion-induced amorphization in indented [110] silicon, J. Mater. Res. 14 (3) (1999) 682–687, https://doi.org/10.1557/JMR.1999.0093.
[141] K. Yamada, C.C. Koch, The influence of mill energy and temperature on the structure of the TiNi intermetallic after mechanical attrition, J. Mater. Res. 8 (6) (1993) 1317–1326, https://doi.org/10.1557/JMR.1993.1317.
[142] D. Yamazaki, S.-I. Karato, High-pressure rotational deformation apparatus to 15 GPa Rev, Sci. Instrum. 72 (11) (2001) 4207–4211, https://doi.org/10.1063/1.1412858.
[143] X.Q. Yan, Z. Tang, L. Zhang, J.J. Guo, C.Q. Jin, Y. Zhang, T. Goto, J.W. McCauley, M.W. Chen, Depressurization Amorphization of Single-Crystal Boron Carbide, Phys. Rev. Lett. 102 (2009), 075505, https://doi.org/10.1103/PhysRevLett.102.075505.
[144] X. Yang, S.P. Coleman, J.C. Lasalvia, W.A. Goddard, Q.i. An, Shear-Induced Brittle Failure along Grain Boundaries in Boron Carbide, ACS Appl. Mater. Interfaces 10 (5) (2018) 5072–5080, https://doi.org/10.1021/acsami.7b16782.
[145] Q. Zeng, A.L. Tonge, K.T. Ramesh, A multi-mechanism constitutive model for the dynamic failure of quasi-brittle materials. Part I: Amorphization as a failure mode, J. Mech. Phys. Solids 130 (2019) 370–392, https://doi.org/10.1016/j.jmps.2019.06.012.
[146] Q. Zeng, A.L. Tonge, K.T. Ramesh, A multi-mechanism constitutive model for the dynamic failure of quasi-brittle materials. Part II: Integrative model, J. Mech. Phys. Solids 131 (2019) 20–42, https://doi.org/10.1016/j.jmps.2019.06.015.
[147] Z. Zhang, Z. Fu, R. Zhang, D. Legut, H. Guo, Anomalous mechanical strengths and shear deformation paths of $Al_2O_3$ polymorphs with high iconicity, RSC Advances. 6 (16) (2016) 12885, https://doi.org/10.1039/C5RA25796D.
[148] S. Zhao, R. Flanagan, E.N. Hahn, B. Kad, B.A. Remington, C.E. Wehrenberg, R. Cauble, K. More, M.A. Meyers, Shock-induced amorphization in silicon carbide, Acta Mater. 158 (2018) 206–213, https://doi.org/10.1016/j.actamat.2018.07.047.
[149] S. Zhao, B. Kad, E. Hahn, L. Chen, Y. Opachi, K. More, B. Remington, C. Wehrenberg, J. LaSalvia, W. Yang, H. Quan, M. Meyers, E. Buzaud, A. Cosculluela, H. Couque, E. Cadoni, Shock-induced Amorphization in Covalently Bonded Solids, EPJ Web Conf. 183 (2018) 03027, https://doi.org/10.1051/epjconf/201818303027.
[150] S. Zhao, Z. Li, C. Zhu, W. Yang, Z. Zhang, D.E.J. Armstrong, P.S. Grant, R. O. Ritchie, M.A. Meyers, Amorphization in extreme deformation of the CrMnFeCoNi high-entropy alloy, Sci. Adv. 7 (5) (2021), https://doi.org/10.1126/sciadv.abb3108.
[151] K. Zheng, C. Wang, Y.-Q. Cheng, Y. Yue, X. Han, Z. Zhang, Z. Shan, S.-X. Mao, M. Ye, Y. Yin, E. Ma, Electron-beam-assisted superplastic shaping of nanoscale amorphous silica, Nature Comm. 1 (2010) 24, https://doi.org/10.1038/ncomms1021.
[152] J. Zhou, R.S. Averback, P. Bellon, Stability and amorphization of Cu–Nb interfaces during severe plastic deformation: molecular dynamics simulations of simple shear, Acta Mater. 73 (2014) 116–127, https://doi.org/10.1016/j.actamat.2014.03.055.
[153] O. Goltrant, P. Cordier, J.C. Doukhan, Planar deformation features in shocked quartz; a transmission electron microscopy investigation, Earth Planet. Sci. Lett. 106 (1991) 103–115, https://doi.org/10.1016/0012-821X(91)90066-Q.
[154] O. Goltrant, H. Leroux, J.C. Doukhan, P. Cordier, Formation mechanisms of planar deformation features in naturally shocked quartz, Phys. Earth Planet. Int. 74 (1992) 219–240, https://doi.org/10.1016/0031-9201(92)90012-K.
[155] A.E. Ringwood, A. Major, Synthesis of majorite and other high pressure garnets and perovskites, Earth Planet. Sci. Lett. 12 (4) (1971) 411–418, https://doi.org/10.1016/0012-821X(71)90026-4.
[156] D. Stöffler, F. Langenhorst, Shock metamorphism of quartz in nature and experiment: I. Basic observation and theory, Meteoritics 29 (1994) 155–181, https://doi.org/10.1111/j.1945-5100.1994.tb00670.x.
[157] P.S. De Carli, J.C. Jamieson, Formation of an amorphous form of quartz under shock conditions, J. Chem. Phys. 31 (6) (1959) 1675, https://doi.org/10.1063/1.1730673.
[158] A.S.J. Koh, H.-P. Lee, Shock-induced localized amorphization in metallic nanorods with strain-rate-dependent characteristics, Nano Letters 6 (10) (2006) 2260–2267, https://doi.org/10.1021/nl061640o.
[159] S.M. Sharma, S.K. Sikka, Pressure induced amorphization of materials, Progress Mater. Sci. 40 (1) (1996) 1–77, https://doi.org/10.1016/0079-6425(95)00006-2.
[160] P. Richet, P. Gillet, Pressure-induced amorphization of minerals: a review, Eur. J. Min. 9 (5) (1997) 907–933, https://doi.org/10.1127/ejm/9/5/0907.
[161] P.R. Okamoto, N.Q. Lam, L.E. Rehn, Physics of crystal-to-glass transformations, Solid State Phys. 52 (1999) 1–135, https://doi.org/10.1016/S0081-1947(08)60018-1.
[162] H. Sowa, The oxygen packings of low-quartz and $ReO_3$ under high pressure, Zeitschrift für Kristallographie 184 (1988) 257–268, https://doi.org/10.1524/zkri.1988.184.3-4.257.
[163] Q. Williams, E. Knittle, R. Reichlin, S. Martin, R. Jeanloz, Structural and electronic properties of $Fe_2SiO_4$-fayalite at ultrahigh pressures: Amorphization and gap closure, J. Geophys. Res. 95 (B13) (1990) 21549–21563, https://doi.org/10.1029/JB095iB13p21549.
[164] D.E. Grady, Adiabatic shear failure in brittle solids, Int. J. Impact Eng. 38 (2011) 661–667, https://doi.org/10.1016/j.ijimpeng.2011.01.001.
[165] B.B. Karki, G.J. Ackland, J. Crain, Elastic instabilities in crystals from *ab initio* stress - strain relations, J. Phys.: Condens. Mat. 9 (1997) 8579–8589, https://doi.org/10.1088/0953-8984/9/41/005.
[166] C.R. Krenn, D. Roundy, J.W. Morris Jr., M.L. Cohen, The non-linear elastic behavior and ideal shear strength of Al and Cu, Mater. Sci. Eng. A 317 (1–2) (2001) 44–48, https://doi.org/10.1016/S0921-5093(01)01178-9.
[167] I.A. Ovid'ko, A.B. Reizis, Effect of elastic distortions on solid-state amorphization at grain boundaries and dislocations, J. Phys. D: Appl. Phys. 32 (1999) 2833–2840, https://doi.org/10.1088/0022-3727/32/22/301.